Bengt Holter

Adaptive Coded Modulation in Spatial and Multiuser Diversity Systems

Doctoral thesis
for the degree of doktor ingeniør

Trondheim, May 2005

Norwegian University of Science and Technology
Faculty of Information Technology, Mathematics
and Electrical Engineering
Department of Electronics and Telecommunications

NTNU
Innovation and Creativity

NTNU
Norwegian University of Science and Technology
Doctoral thesis
for the degree of doktor ingeniør
Norwegian University of Science and Technology
Faculty of Information Technology, Mathematics and Electrical Engineering
Department of Electronics and Telecommunications

© Bengt Holter

ISBN 82-471-6966-5 (printed vers.)
ISBN 82-471-6965-7 (electronic vers.)
ISSN 1503-8181

Doctoral theses at NTNU, 2005:49

Printed by NTNU-trykk

Abstract

This thesis consists of five included papers plus an introduction. The majority of the papers are devoted to performance analysis of an adaptive coded modulation (ACM) scheme based on multidimensional trellis codes. Primarily, single-user systems exploiting spatial diversity are analysed, but results are also presented for a multiuser system exploiting multiuser diversity.

The performance of the ACM scheme is evaluated for slowly flat-fading channels. When spatial diversity is exploited at the receiver end only, the analysis is focused on two different combining techniques: *maximum ratio combining* (MRC) and *switched combining*. A multiple-input multiple-output (MIMO) diversity system is also considered, in which case the combined effect of both transmit and receive diversity is realized by using space-time block coding at the transmitter.

For wireless systems using spatial diversity, it is of interest to employ measures which can capture and quantify the performance improvement related to a reduced fading level. In this thesis, a measure called the amount of fading (AF) is used to characterize the behavior of the error rate curve at a high signal-to-noise ratio (SNR). In particular, closed-form expressions for the AF at the output of a MIMO diversity system are provided, and it is shown that for a constant correlation model, the average symbol error probability at high SNRs may be expressed in terms of the AF.

Finally, a set of switched multiuser access schemes are proposed based on switched diversity algorithms originally devised to select between antennas in a spatial diversity system. ACM is used on each selected link to ensure a high spectral efficiency of the system.

Preface

This dissertation is submitted in partial fulfillment of the requirements for the degree of *doktor ingeniør* at the Department of Electronics and Telecommunications, Norwegian University of Science and Technology (NTNU). My advisors have been Professor Geir E. Øien at the Department of Electronics and Telecommunications, NTNU, and Professor Kjell J. Hole at the Department of Informatics at the University of Bergen (UiB). The studies have been carried out in the period from January 2001 to February 2005. The work includes the equivalent of a year of full-time course studies.

As a doctoral student, I have had the opportunity to visit two research groups abroad. From May 2003 to March 2004, I was part of the Communication Theory Group headed by Professor Helmut Bölcskei at the Swiss Federal Institute of Technology (ETH) in Zürich, Switzerland. In February 2004, I visited the research group of Professor Mohamed-Slim Alouini at the University of Minnesota, Minneapolis, USA.

The work has been funded by a scholarship from the Research Council of Norway, via the project *Bandwidth-Efficient and Adaptive Transmission Schemes for Wireless Multimedia Communications* (BEATS), and SINTEF ICT.

Acknowledgements

I would like to thank my supervisors Professor Geir E. Øien and Professor Kjell J. Hole for their advice and valuable comments. Their enthusiasm and support inspired me to become a doctoral student. I am grateful to Professor Helmut Bölcskei, for letting me be a part of the Communication Theory Group at ETH in Zürich. I initiated most of my work during this stay. From the Communication Theory Group, I want to thank Ph.D. student Markus Gärtner for helping me with a lot of practical matters.

In the last four years, I have had the pleasure of meeting Professor Mohamed-Slim Alouini several times. I would like to thank him for many inspiring and fruitful discussions on topics of common interest. I want to thank my colleagues at NTNU and SINTEF ICT. I have bothered several of you with some peculiar questions, and I have really appreciated your efforts on helping me with your insights. In particular, I want to thank Ola Jetlund and Duc Van Duong for contributing to new insights through inspiring discussions. I am grateful to my employer SINTEF ICT for financial support and my former research director Erik Olsen for letting me pursue a doctoral degree.

During my visit to the University of Minnesota in February 2004, I shared office with Henrik Holm. I would like to thank him and his wife Basobi for their hospitality and for letting me spend two nights at their house in Lakeville, a southern suburb of Minneapolis. It was freezing cold when I was in Minneapolis, so instead of sleeping in thin blankets at the hotel, it was really nice sleeping in a Norwegian style bed for two nights.

In my spare time, I am eager to play the trombone. In Zürich, I joined two orchestras: the wind band *Stadtmusik Zürich* and the *Nota-Bene Symphony Orchestra*. I want to thank Ralph Tonezzer, Markus Hahn, and Marco Lucarelli from the symphony orchestra. Upon my wish, we met twice to play trombone quartets, and we all enjoyed it very much. From Stadtmusik Zürich, I want to thank the entire trombone section: Hans-Peter Meier, Markus Strolz, Viola Kummer, Patrick Isker, and René Isker. They were all very helpful to me, translating the swiss-german comments from the conductor into either german or english.

I want to thank my family for all the support during the last four years. In particular, my mother Gerd, for her enthusiasm and positive attitude, and my identical twin brother Atle, for his knowledge in signal processing conveyed to me during our (almost) daily phone calls. Finally, I want to express my deepest and sincere thanks to my common-law spouse Ingrid for all her love, patience, and support.

Trondheim, February 2005
Bengt Holter

Contents

Contents v

Figures ix

Tables xv

I Introduction 1

References 25

II Included papers 31

A Performance Analysis of a Rate-Adaptive Dual-Branch Switched Diversity System 33

1 Introduction 37
2 System and channel model 39
3 ASE and BER analysis 40
4 Maximizing the ASE 43
5 Comparison with MRC and SC 44
6 Impact of branch correlation 45
7 Impact of time delay 47
  Uncorrelated branches 49
  Correlated branches 50
8 Numerical results 51
9 Conclusion 53

References 59

B Impact of Spatial Correlation on Adaptive Coded Modulation Performance in Rayleigh Fading 63
1 Introduction 67
2 System and channel model 68
3 Statistics of the combined CSNR 70
4 Diversity order and coding gain 74
Exact PDF 75
Approximate PDF 76
5 Linear pilot-symbol assisted channel prediction 77
6 Correlation and ratio coefficient 78
Correlation coefficient 78
Ratio coefficient 80
7 ASE and BER analysis 80
8 Numerical results 84
9 Conclusion 86

References 97

C Limitations in Spectral Efficiency of a Rate-Adaptive MIMO System Utilizing Pilot-Aided Channel Prediction 101
1 Introduction 105
2 System model 105
3 Channel model 106
SIMO channel model 106
MIMO channel model 107
4 BER and ASE analysis 108
5 Numerical results 113
6 Conclusion 113

References 119

D On the Amount of Fading in MIMO Diversity Systems 121
1 Introduction 125
2 Statistics of the combined fading power 127
3 Amount of fading 128
4 AF_{con} and its relation to the average SER at high SNR . . . 132
5 Numerical results 136
6 Conclusion 137

References 141

E **Multiuser Switched Diversity Transmission** **145**
1 Introduction 149
2 System and channel model 150
3 ASE and BER analysis 151
4 Multiuser access schemes 151
Scan-and-wait transmission (SWT) 152
Switch-and-examine transmission (SET) 153
SET with post-selection (SETps) 154
Selection combining transmission (SCT) 155
5 Average feedback load 156
Trade-off between ASE performance and AFL 156
6 Average waiting time 157
7 Numerical results 157
8 Conclusion 158

References **165**

III Appendices **167**

1 The generalized Marcum Q-function **169**

References **171**

2 Useful integration rules **173**

References **175**

3 Detailed derivation of the expression in (B.35) **177**

References **181**

4 ASE and average BER under idealized assumptions **183**

References **187**

5 Comments on the results in [1] **189**

References **191**

6 Proof of the Amount of Fading expression in (D.11) **193**

7 An alternative expression for the determinant of a constant correlation matrix 195

References 197

8 Proofs of statistical results presented in Paper E 199

References 203

9 The optimal weights of an MRC receiver by means of an eigenfilter approach 205

References 211

Figures

1.1 The SNR range is split into $N+1$ bins. When the instantaneous SNR falls in the lowest interval, an outage occurs; whereas in the upper N intervals, codes with rates $\{R_n\}_{n=1}^{N}$ are employed. 8
1.2 QAM constellation with 256 symbols. The symbol constellations with 4, 8, 16, 32, 64, and 128 signal points are nested within the 256-QAM constellation. The crosses constitute the symbol constellation with 8 signal points. 9
1.3 The boxes are BER estimates generated by software simulations, whereas the solid lines are estimates obtained from (1.3). The labels denote the number of symbols in the QAM signal constellations utilized by the four-dimensional trellis codes. . . . 10
1.4 ACM system with pilot-symbol-assisted channel estimation (for coherent detection) and prediction (for transmitter adaptation). 13

A.1 The SNR range is split into $N+1$ bins. When the instantaneous SNR falls in the lowest interval, an outage occurs; whereas in the upper N intervals, a code with rate R_n is employed. 54
A.2 The size of $R_q - \mathcal{A}_1$ for $m = 1$, governing the sign of the gradient in (A.12). 55
A.3 ASE as a function of $\overline{\gamma}$ when operating on i.i.d. Rayleigh fading channels. For SSC, $\gamma_T = \gamma_T^*$ for each value of $\overline{\gamma}$. 55
A.4 Switching threshold γ_T^*, maximizing the ASE over all fading bins, as a function $\overline{\gamma}$ and the Nakagami-*m* fading parameter. . 56
A.5 Average BER as a function of $\overline{\gamma}$ and the Nakagami-*m* fading parameter. For SSC, $\gamma_T = \gamma_T^*$ for each value of $\overline{\gamma}$. 56
A.6 ASE as a function of $\overline{\gamma}$ and ρ_s when operating on identically distributed Rayleigh fading channels. In the single branch case, ASE $= \mathcal{A}_1$. 57
A.7 Average BER as a function of $\overline{\gamma}$ and ρ_s when operating on identically distributed Rayleigh fading channels. In the single branch case, $\overline{\text{BER}} = \mathcal{B}_1/\mathcal{A}_1$. 57

A.8 Average BER as a function of normalized time delay $f_D\tau$ and the Nakagami-m fading parameter for $\rho_s = 0$, $\overline{\gamma} = 20$ dB and $\gamma_T = 17.6$ dB. 58

A.9 Average BER as a function of normalized time delay $f_D\tau$ for $\rho_s = \{0, 0.5\}$, $\overline{\gamma} = 20$ dB, and $\gamma_T = 17.6$ dB. In all cases where $m \in \{2, 4\}$, the angle of arrival of the LOS component is assumed to be in the direction of motion, i.e. $\theta_0 = 0$. In the single branch case, $\overline{\mathrm{BER}} = \mathcal{B}_{1,\rho_t} / \mathcal{A}_1$. 58

B.1 ACM system with pilot-symbol-assisted channel estimation (for coherent detection purposes) and prediction (for transmitter adaptation purposes). 87

B.2 The CSNR range is split into $N + 1$ bins. When the instantaneous CSNR falls in the lowest interval, an outage occurs; whereas in the upper N intervals, a code with rate R_n is employed. 87

B.3 Comparison of the exact and approximate PDFs for γ when $H = 2$ and the system is operating on identically distributed and spatially correlated Rayleigh fading channels ($\overline{\gamma} = 1$). . . 88

B.4 Comparison of the exact and approximate PDFs for γ when $H = 4$ and the system is operating on identically distributed and spatially correlated Rayleigh fading channels ($\overline{\gamma} = 1$). **Top subfigure**: constant correlation model. **Bottom subfigure**: exponential correlation model. 88

B.5 Diversity and coding gain realized at high CSNR for a system operating on identically distributed spatially correlated Rayleigh fading channels, using BPSK transmission only. The abbreviations con and exp in the legends of both subfigures are related to results obtained with a constant and exponential correlation model, respectively. **Top subfigure**: G_d in (B.21) obtained with the approximate PDF is depicted. It should be related to G_d in (B.17), obtained with the exact PDF, in which case $G_d = H$. **Bottom subfigure**: Expressions for G_c in (B.18) and (B.22) are depicted for $H = 4$. 89

B.6 Average BER and ASE as a function $\overline{\gamma}_h$ when using the exact and approximate PDF ($H = 2$ and $\rho_{12} = \rho_{21} = \rho_s = 0.2$ in (4.2)). The assumptions are perfect channel knowledge and no time delay on the feedback channel. 90

B.7 Average BER and ASE as a function $\overline{\gamma}_h$ when using the exact and approximate PDF ($H = 2$ and $\rho_{12} = \rho_{21} = \rho_s = 0.7$ in (4.2)). The assumptions are perfect channel knowledge and no time delay on the feedback channel. 90

B.8 Average BER and ASE as a function $\overline{\gamma}_h$ when using the exact and approximate PDF with a constant correlation model ($H = 4$ and $\rho_{ij} = \rho_s = 0.7$ in (4.2)). The assumptions are perfect channel knowledge and no time delay on the feedback channel. 91

B.9 Average BER and ASE as a function $\overline{\gamma}_h$ when using the exact and approximate PDF with an exponential correlation model ($H = 4$ and $\rho_{ij} = \rho_s^{|i-j|}$ in (4.2), with $\rho_s = 0.7$). The assumptions are perfect channel knowledge and no time delay on the feedback channel. 91

B.10 Average BER as a function $\overline{\gamma}_h$ and normalized time delay on the feedback channel when $H = 4$ and the system operating on uncorrelated Rayleigh fading channels. The pilot symbol spacing $L = 10$, and the prediction filter length is $K = 1000$. 92

B.11 Average BER as a function $\overline{\gamma}_h$ and normalized time delay on the feedback channel when $H = 4$ and the system is operating on exponentially correlated Rayleigh fading channels ($\rho_s = 0.7$). The pilot symbol spacing $L = 10$, and the prediction filter length is $K = 1000$. 92

B.12 Regions where the system performance is acceptable, plotted for $H = \{2, 4\}$, $L = 10$, $K = 1000$, and $\rho_s = \{0, 0.2, 0.7\}$. The curves indicate the largest delay that is allowed in order to achieve the BER requirements for a given average CSNR $\overline{\gamma}_h$. Thus, the performance is acceptable for each point specified by a CSNR/delay combination that is below and to the right of the curves. 93

B.13 Zero-delay ASE compared to the channel capacity (optimal rate adaptation with constant transmit power) [30, Sec. IV] for $H = 2$ and $\rho_s = \{0, 0.7\}$. 94

B.14 Zero-delay ASE compared to the channel capacity (optimal rate adaptation with constant transmit power) [30, Sec. IV] for $H = 4$ and $\rho_s = \{0, 0.7\}$. 94

B.15 ASE as a function of $\overline{\gamma}_h$ and normalized feedback time delay when $L = 10$, $H = 2$, and $\rho_s = 0.7$. The contour line divides the ASE into a relevant part where the BER constraints are fulfilled (to the left of the contour line) and an irrelevant part where the BER constraints are violated (to the right of the contour line). The prediction filter length is $K = 1000$. 95

C.1 Transmitter 114

C.2 Receiver 114

C.3 Average BER as a function of feedback delay and of expected subchannel CSNR. $\kappa = 5$ antennas are utilized (1×4 system) and the pilot symbol spacing is $L = 7$. The prediction filter length is $K = 1000$. 115

C.4 Average BER as a function of feedback delay and of expected subchannel CSNR. $\kappa = 4$ antennas are utilized (2×2 system with STBC G_2) and the pilot symbol spacing is $L = 7$ ($L_b = 8$). The prediction filter length is $K = 1000$. 115

C.5 Average BER as a function of feedback delay and of expected subchannel CSNR. $\kappa = 6$ antennas are utilized (3×3 system with STBC H_3) and the pilot symbol spacing is $L = 7$ ($L_b = 11$). The prediction filter length is $K = 1000$. 116

C.6 Average spectral efficiency as a function of expected subchannel CSNR [dB], plotted for various L and a normalized feedback time delay (symbol duration normalized with respect to maximum Doppler spread) of 0.25. For the 2×2 system, the STBC G_2 is employed. For the 3×3 system, the STBC H_3 is employed. 117

D.1 Numerical comparison of closed form expressions for the determinant of a constant correlation matrix $\mathbf{R}$. **Left figure**: $\det(\mathbf{R}) = (1-x)^{L-1}(1+x(L-1))$. **Right figure**: $\det(\mathbf{R}) = betacdf(1-x, L-1, 2)$. 138

D.2 AF$_{con}$ (in dB) as a of function the power correlation coefficient $\rho = \rho_t = \rho_r$ for SIMO, MISO, and MIMO diversity systems ($n_T \times n_R$) operating on identically distributed Rayleigh fading channels: (a) $(1 \times n_R)$; (b) $(2 \times n_R)$; (c) $(3 \times n_R)$; (d) $(4 \times n_R)$. . 138

D.3 **Top figure**: Exact average SER (dashed lines) and approximate average SER at high SNR (solid lines) for a 3×3 MIMO diversity system operating on identically distributed Rayleigh fading channels (constant correlation models at each end of the MIMO link). A BPSK modulation scheme is utilized. **Bottom figure**: Relative (right) shift (in dB) of the SER benchmark curve presented in the top figure as a function of ρ_r when $\rho_t = 0$. Using the top x-axis as a reference, the AF realized by the 3×3 MIMO diversity system is compared (in percentage) to the AF of a single Rayleigh fading channel (100% reduction represents the non-fading AWGN channel). 139

D.4 **Top figure**: Exact average SER (dashed lines) and approximate average SER at high SNR (solid lines) for a 3×3 MIMO diversity system operating on identically distributed Rayleigh fading channels (constant correlation models at each end of the MIMO link). A BPSK modulation scheme is utilized. **Bottom figure**: Relative (right) shift (in dB) of the SER benchmark curve presented in the top figure as a function of ρ_r when $\rho_t = 0.5$. Using the top x-axis as reference, the AF realized by the 3×3 MIMO diversity system is compared (in percentage) to the AF of a single Rayleigh fading channel (100% reduction represents the non-fading AWGN channel). 140

E.1 ASE (unconstrained optimization) for the SCT, SETps, SET, and SWT access schemes when the multiuser system is assumed to be operating on i.i.d. Rayleigh fading channels with $\overline{\gamma} = [5, 15, 25]$ dB. 160

E.2 Optimal thresholds γ_T maximizing the ASE subject to no AFL constraints (unconstrained optimization). The multiuser system is assumed to be operating on i.i.d. Rayleigh fading channels with $\overline{\gamma} = 15$ dB. 160

E.3 AFL (unconstrained optimization) for the SCT, SETps, SET, and SWT access schemes. For reference purposes, the solid line visualizes the (linear) upper bound for the constraint AFL $\leq 0.3K$. The multiuser system is assumed to be operating on i.i.d. Rayleigh fading channels with $\overline{\gamma} = 15$ dB. 161

E.4 AFL for the SCT, SETps, SET, and SWT access schemes when AFL $\leq 0.3K$. When the constraint cannot be met, AFL $= 0$ for simplicity. The multiuser system is assumed to be operating on i.i.d. Rayleigh fading channels with $\overline{\gamma} = 15$ dB. 161

E.5 ASE realized by the SETps access scheme when the AFL is upper bounded by AFL $\leq \alpha K$. When the constraint cannot be met, ASE $= 0$ for simplicity. The multiuser system is assumed to be operating on i.i.d. Rayleigh fading channels with $\overline{\gamma} = 15$ dB. . 162
E.6 ASE realized by the SET access scheme when the AFL is upper bounded by AFL $\leq \alpha K$. When the constraint cannot be met, ASE $= 0$ for simplicity. The multiuser system is assumed to be operating on i.i.d. Rayleigh fading channels with $\overline{\gamma} = 15$ dB. . 162
E.7 ASE realized by the SWT access scheme when the AFL is upper bounded by AFL $\leq \alpha K$. When the constraint cannot be met, ASE $= 0$ for simplicity. The multiuser system is assumed to be operating on i.i.d. Rayleigh fading channels with $\overline{\gamma} = 15$ dB. . 163
E.8 Average waiting time (AWT) for the SWT access scheme. When the constraint cannot be met, AWT $= 0$ for simplicity (when AFL $\leq 0.1K$, AWT $= 0$ for $K \leq 12$). The multiuser system is assumed to be operating on i.i.d. Rayleigh fading channels with $\overline{\gamma} = 15$ dB. 163

5.1 Comparison of the exact and approximate PDFs in [1, Fig. 1], including corrected results based on a complex representation of the covariance matrix in [1, Eq. (9)]. The curves are obtained for $\overline{\gamma} = 1$ and $m = 1$. 190

Tables

A.1 PDF and CDF of the SNR per symbol γ for a single Nakagami-m fading channel 54

A.2 Parameters a_n and b_n with thresholds γ_n for $\text{BER}_0 = 10^{-4}$. . . 54

B.1 Expressions for ψ and θ for constant and exponential correlation models 87

C.1 Orthogonal designs for STBC 111

Abbreviations

ACM	Adaptive coded modulation
AF	Amount of fading
AFL	Average feedback load
ASE	Average spectral efficiency
AWGN	Additive white Gaussian noise
AWT	Average waiting time
BER	Bit-error-rate
BPSK	Binary phase-shift keying
BS	Base station
CDF	Cumulative distribution function
CF	Characteristic function
CSI	Channel state information
CSNR	Channel signal-to-noise ratio
dB	Decibel
DD	Decision-directed
LOS	Line-of-sight
MGF	Moment generating function
MIMO	Multiple-input multiple-output
MISO	Multiple-input single-output
M-PSK	M-ary phase-shift keying
MRC	Maximum ratio combining
NLOS	Non-line-of-sight
PDF	Probability density function
PMF	Probability mass function
QAM	Quadrature amplitude modulation
RV	Random variable
SC	Selection combining
SCT	Selection combining transmission
SEC	Switch-and-examine combining

SER	Symbol-error-rate
SET	Switch-and-examine transmission
SETps	Switch-and-examine transmission with post-selection
SIMO	Single-input multiple-output
SINR	Signal-to-interference plus noise ratio
SNR	Signal-to-noise ratio
SSC	Switch-and-stay combining
STBC	Space-time block coding
SWT	Scan-and-wait transmission
TDM	Time division multiplexed

Part I

Introduction

Introduction

In order to achieve high-speed transmission of data on a wireless channel, a reliable and spectrally efficient transmission scheme is needed. However, the hostility of the wireless channel makes this a challenging task, since signals tend to propagate along different paths due to reflection, scattering, and diffraction from obstructing objects. The received signal will then be a sum of randomly delayed signal components which will add either constructively or destructively, causing rapid fluctuations in the received signal level. This is called multipath fading, and through the years, it has been perceived as a phenomenon with detrimental effects on spectral efficiency. Based on this perception, wireless transmission schemes have traditionally been designed for the worst-case scenario by focusing on enabling the system to perform acceptably even in deep fading conditions. With such a design principle, spectral efficiency is sacrificed for link reliability.

A design principle focusing more on spectral efficiency is rate-adaptive transmission, where the basic concept is to exploit and track the time varying characteristics of the wireless channel to transmit with as high information rate as possible when the channel quality is good, and to lower the information rate (and trade it for link reliability) when the channel quality is reduced [1–5]. With such a transmission scheme, a feedback channel is required, on which the receiver reports channel state information (CSI) to the transmitter. Based on the reported CSI, the transmitter can make a decision on which rate to employ for the next transmission period. In particular, the transmitter may choose to select symbols from the biggest constellation meeting a predefined bit-error-rate (BER) requirement, to ensure that the spectral efficiency is maximized for an acceptable (target) BER. A promising method is to vary the constellation size and the channel coding scheme (error control) according to the channel conditions, in which case a rate-adaptive transmission scheme is called *adaptive coded modulation* (ACM) [6, 7].

Throughout this thesis, slowly flat-fading channels are assumed. The notion of a slow fading channel is related to the channel coherence time T_c, which is a measure of the time period where the fading process is correlated [8]. A fading process is characterized as slow if the symbol time period T_s is smaller than T_c, in which case a particular fading level will affect several successive symbols (block fading). In addition, if the fading process affects all the spectral components within a certain bandwidth in a similar manner, the fading is said to be frequency-flat. This is the case for narrowband systems, in which case the bandwidth B [Hz] of the transmitted signal is much smaller than the coherence bandwidth B_c [Hz] of the channel. The coherence bandwidth is a measure of the frequency range over which the fading process is correlated [8]. Since all the frequency components of a signal transmitted on a flat-fading channel are affected in the same way, it will not be distorted in frequency. That is, the flat-fading channel represents a multiplicative channel rather than a convolutional channel, and the complex baseband representation of the channel response may be written simply as a complex number $z = \alpha \cdot e^{-\jmath\beta}$. All the frequencies within the signal bandwidth will then be subjected to the same attenuation α (also known as fading amplitude or fading envelope) and the same phase shift β. When evaluating the performance of digital communication techniques over slowly flat-fading channels, α may be viewed as a random variable (RV), where the probability density function (PDF) of α is dependent on the radio propagation environment [8].

The Rayleigh distribution is frequently used when there is no line-of-sight (LOS) between the transmitter and the receiver. In the presence of a LOS component, a Rice distribution or a Nakagami-m distribution may be applied. The two distributions are closely related, but due to the simplicity of the Nakagami-m distribution, it is often preferred, as it frequently leads to closed-form analytical expressions and insights which are difficult to obtain with the Rice distribution [9]. For a Nakagami-m fading model, the PDF of α is given by [10]

$$f_\alpha(\alpha) = \frac{2m^m \alpha^{2m-1}}{\Omega^m \Gamma(m)} e^{-\frac{m\alpha^2}{\Omega}}; \;\; \alpha \geq 0, \tag{1.1}$$

where m is the Nakagami-m fading parameter which ranges from $1/2$ (half Gaussian model) to ∞ (additive white Gaussian noise (AWGN) channel), $\mathcal{E}\{\alpha^2\} = \Omega$, and $\Gamma(\cdot)$ is the gamma function [11, Eq. (8.310)].[1] A nice feature of the Nakagami-m distribution is that the Rayleigh distribution is included as a special case $(m = 1)$. The Nakagami-m distribution often gives the best fit to land-mobile and indoor-mobile multipath propagation environments [8].

---

[1] $\mathcal{E}\{\cdot\}$ denotes the statistical average.

A wireless system may be classified in terms of the number of antennas used for transmission and reception. The most traditional configuration uses a single transmit antenna and a single receive antenna, in which case the system is defined as a single-input single-output (SISO) system. With multiple antennas at the receiver, the system is classified as a single-input multiple-output (SIMO) system. Similarly, with multiple transmit antennas and a single receive antenna, the system is a multiple-input single-output (MISO) system. Finally, if multiple antennas are employed at both sides of the link, the system is classified as a multiple-input multiple-output (MIMO) system. Traditionally, multiple antennas have been employed at the receiver end only, to combat the effects of multipath fading. This technique is known as *spatial diversity*, and it refers to the basic principle of picking up multiple copies of the same signal at different locations in space. A potential diversity gain is achieved and maximized if the antennas are sufficiently separated such that the fading characteristics are independent. With the advent of space-time codes, diversity gains may also be achieved in MISO and MIMO systems, irrespective of the transmitter having channel knowledge or not [12, 13].

Transmission schemes for MIMO systems may in general be divided into two categories: rate maximization schemes and diversity maximization schemes. MIMO systems within the two categories are known as *spatial multiplexing* systems and *MIMO diversity* systems, respectively [14]. A spatial multiplexing system utilizes the channel to provide increased spectral efficiency, by transmitting independent streams of data from each transmit antenna. In a rich scattering environment, each transmit antenna induces a different spatial signature at the receiver. The receiver exploits these signature differences to separate the individual data streams. An important information-theoretic result is that with spatial multiplexing, capacity scales linearly, rather than logarithmically, with increasing signal-to-noise ratio (SNR)[2] [15–17]. In addition, this increase in capacity comes at no extra bandwidth or power consumption.

A MIMO diversity system uses the channel to provide increased link reliability by jointly encoding the individual data streams to protect the data from errors caused by multipath fading. This is achieved by using a signal processing technique called space-time block coding (STBC) [12, 13]. Space-time block codes are designed to achieve the maximum diversity order for a given number of transmit and receive antennas, subject to the constraint of having a simple decoding algorithm. As such, they incur a loss in capacity because they convert the MIMO matrix channel into a scalar AWGN channel whose capacity is smaller than the true channel capacity [18].

---

[2] In this thesis, SNR and CSNR (channel-signal-to-noise ratio) are interchangeably used as abbreviations for the signal-to-noise ratio. SNR is normally used, but CSNR is used in two of the included papers, for reference purposes.

Diversity schemes are usually classified according to the type of combining technique employed at the receiver. In the absence of interference, *maximum ratio combining* (MRC) [19] is the optimal combining scheme for any fading distribution, in the sense that it maximizes the received SNR. As such, it may be viewed as the stochastic counterpart of a matched filter [20]. In an MRC receiver, the output signal is the coherent sum of the signals from all the branches. In particular, the complex signal amplitudes on all the branches are co-phased and weighted according to their individual strength such that the SNR of the combined signal is maximized. In Appendix 9, the optimal complex weights (amplitude and phase) of an MRC receiver are derived by means of an eigenfilter approach, which was originally proposed in [21]. The optimality of the MRC receiver comes at the expense of complexity, since for coherent detection, complete knowledge of all channel parameters[3], and separate receiver RF[4]/analog chains on all the branches are needed [8].

A less complex diversity scheme is *selection combining* (SC) [8, Sec. 9.7], where only a single branch and not the coherent sum is selected for further processing. In particular, an SC receiver monitors the instantaneous SNR on all the branches and selects the branch with the highest SNR. As a consequence, only a single receiver chain is needed for its implementation. However, since simultaneous and continuous monitoring of the channel state on all the branches is required, an SC receiver is often replaced by a *switched combining* receiver [8, Sec. 9.8]. In this case, the receiver is not always connected to the best branch, but is connected to a particular branch as long as the received SNR of that branch do not drop below a predefined threshold. If this happens, the receiver simply switches to another branch. With such an approach, the receiver at any time only needs to monitor the channel state of the currently selected branch. This contributes to reduce the complexity in comparison to the SC combiner, but it comes at the expense of a certain performance loss.

All the spatial diversity combining techniques mentioned above have in common that the diversity gain arises from independent signal paths received by multiple antennas. Another type of diversity is *multiuser diversity* [22, 23]. This type of diversity is naturally inherent in systems where several users are communicating with a base station (BS) on a shared frequency band. The diversity is attributed to the fact that for a given moment in time, different users usually have different channel conditions. In this situation, the total system throughput can be maximized by only letting the user having the best channel quality transmit at any given time [24, 25]. However, repeatedly scheduling the best user might not be a fair strategy to communicate on a shared frequency band, since the same favorable user might end up being selected every time. Hence, scheduling users in a multiuser system by exploiting multiuser diversity also involve fairness and latency issues. In addition, the BS needs feedback from the users to make a decision on which user to schedule for the next transmission period. If all the users are to report their channel status on a regular basis, it will contribute to drain the terminal batteries more rapidly and generate a lot of overhead traffic in the system. As a remedy, recent papers on scheduling and multiuser diversity are suggesting scheduling methods which reduce the amount of feedback information by letting the BS make a decision based on a predefined set of channel thresholds [26–29]. In general, this means that for a given moment in time, only a single user or a small group of users which can report channel conditions above a certain level are allowed to report it to the BS. The total number of users can be divided into smaller groups where users within a particular group exhibit almost similar channel conditions. When a certain group of users is addressed by the BS, users within that group are able to compete for the channel on equal terms.

---

[3] For flat-fading channels, the amplitude and phase of the complex channel amplitudes on all the branches must be known.

[4] Radio frequency

Recently, it has been reported that additional use of spatial diversity in multiuser systems counteracts the performance gain obtained by multiuser transmission. In [30], it is argued that multiuser diversity with no spatial diversity outperforms schemes that employ both multiuser diversity and spatial diversity. However, in [31], it is commented that, if properly exploited, spatial diversity really do increase and not decrease the total diversity gain in a system that takes advantage of both spatial and multiuser diversity.

Adaptive coded modulation

A major part of this thesis is devoted to performance analysis of an ACM scheme based on multidimensional trellis codes originally designed for AWGN channels [7, 32]. Primarily, the analysis is focused on single-user systems exploiting spatial diversity, but results are also obtained for a multiuser system exploiting multiuser diversity. In the following, a brief summary of literature related to the ACM scheme in question is presented,

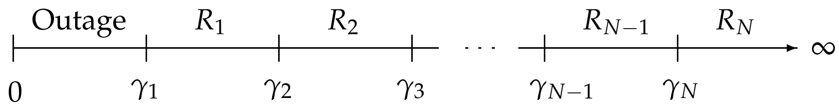

FIGURE 1.1: The SNR range is split into $N+1$ bins. When the instantaneous SNR falls in the lowest interval, an outage occurs; whereas in the upper N intervals, codes with rates $\{R_n\}_{n=1}^{N}$ are employed.

along with relevant details of the ACM scheme.

In [7] and [32, Ch. 2], the ACM scheme based on multidimensional trellis codes is presented along with performance merits when applied on a SISO system operating on a Nakagami-*m* fading channel. Perfect channel knowledge at the receiver and perfect CSI at the transmitter are assumed (zero-error feedback channel with no time delay). A set of N $2G$-dimensional trellis codes are employed. Each code is based on quadrature amplitude modulation (QAM) signal constellations of varying size $M_n = 2^{k_n}$, where $n = \{1, 2, \ldots, N\}$ and k_n is some positive integer. Rate adaptation is performed by splitting the SNR range into $N+1$ fading regions (bins) as depicted in Figure 1.1. Each of the N codes is then assigned to operate within a particular fading region, except for the leftmost bin. The SNR thresholds in the set $\{\gamma_n\}_{n=1}^{N}$ are selected such that each code operates below a predefined target BER. When the instantaneous SNR γ falls within the fading region $\gamma_n \leq \gamma < \gamma_{n+1}$, the associated CSI, i.e. the fading region index n, is sent back to the transmitter. The transmitter then adapts its transmission rate and coding scheme by transmitting with a code realizing a spectral efficiency of R_n (measured in bits/s/Hz). The spectral efficiencies of the applied codes are organized such that $R_1 < R_2 < \ldots < R_N$. This enables the system to transmit with high spectral efficiency when the instantaneous SNR is high, and to reduce the spectral efficiency as the SNR decreases. The target BER is not achieved when $\gamma < \gamma_1$, so no information is transmitted when γ falls into the leftmost interval $0 \leq \gamma < \gamma_1$ (outage). During this situation, the information must be buffered at the transmitter.

In general, for a $2G$-dimensional trellis code, where $G \in \{1, 2, \ldots\}$, the spectral efficiency R_n of code n is obtained as follows. The encoder for code n accepts $p = G \log_2(M_n) - 1$ information bits at each time index $k = GT_s$. The encoder generates $p + 1 = G \log_2(M_n)$ coded bits which specify G transmittable QAM symbols from the nth constellation with M_n symbols. Since G (two-dimensional) QAM symbols generated at each time index k can be viewed as *one* $2G$-dimensional symbol, the generated code is

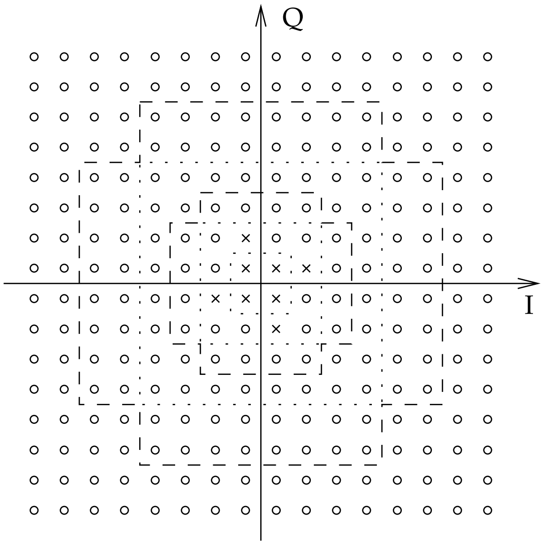

FIGURE 1.2: QAM constellation with 256 symbols. The symbol constellations with 4, 8, 16, 32, 64, and 128 signal points are nested within the 256-QAM constellation. The crosses constitute the symbol constellation with 8 signal points.

said to be a $2G$-dimensional trellis code. As a result, p information bits are transmitted within GT_s uses of the channel. The information rate for code n may then be expressed as $R_n = (p/(GT_s))/B$. Assuming ideal Nyquist pulses (transmission with no intersymbol interference), we have $B = 1/T_s$, in which case the spectral efficiency of code n is equal to $R_n = k_n - 1/G$ [bits/s/Hz]. In this thesis, $N = 8$ four-dimensional trellis codes are used, i.e. $G = 2$. These codes are based on eight nested QAM signal constellations with $M_n = 2^{k_n} \in \{4, 8, 16, 32, 64, 128, 256, 512\}$ signal points for $k_n = n + 1$ and $n = 1, 2, \ldots, 8$ (see Figure 1.2).[5] Hence, the associated spectral efficiencies are $R_n = \{1.5, 2.5, \ldots, 8.5\}$.

The *average* spectral efficiency (ASE) is obtained as the weighted sum of the spectral efficiencies $\{R_n\}_{n=1}^{N}$

$$\text{ASE} = \sum_{n=1}^{N} R_n \cdot P_n, \tag{1.2}$$

where the weight factor P_n is the probability that code n is used. Since this

---

[5] The QAM constellation with 512 symbols is omitted from Figure 1.2 due to space and visibility requirements.

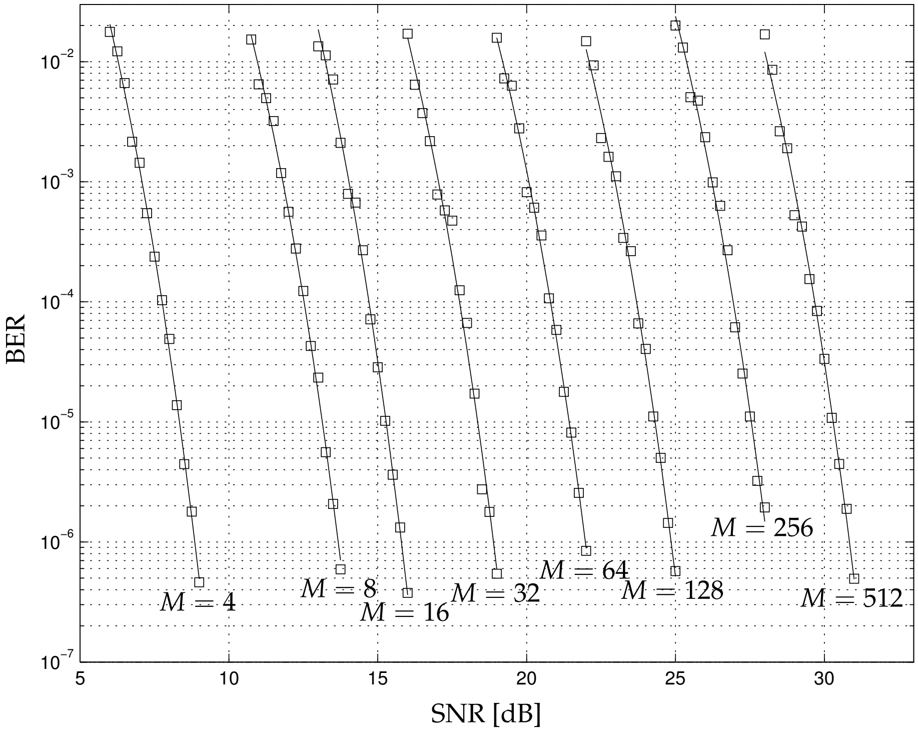

FIGURE 1.3: The boxes are BER estimates generated by software simulations, whereas the solid lines are estimates obtained from (1.3). The labels denote the number of symbols in the QAM signal constellations utilized by the four-dimensional trellis codes.

is equivalent to the probability that the instantaneous SNR falls within a particular fading bin n, the thresholds $\{\gamma_n\}_{n=1}^{N}$ must be known. In [7, Eq. (9)], it is argued that the BER when code n is applied on an AWGN channel, as a function of the SNR γ—denoted BER_n—may be approximated by the expression

$$\text{BER}_n \approx a_n \cdot e^{-\frac{b_n \gamma}{M_n}}, \tag{1.3}$$

where a_n and b_n are code-dependent constants found by least square curve fitting to simulated data on AWGN channels of varying SNRs. In Figure 1.3 [32, Fig. 2.2], the BER performance of the individual codes are depicted along with the results of the curve fitting technique.[6] From the curve fitting technique and for a given target BER—denoted BER_0—the thresholds

---

[6] According to [32], the BER results depicted in Figure 1.3 are obtained when the path length of the Viterbi decoder is 9.

$\{\gamma_n\}_{n=1}^N$ are obtained by assuming equality in (1.3), in which case

$$\begin{array}{rcll} \gamma_n & = & (M_n K_n)/b_n & n = 1, 2, \ldots, N \\ \gamma_{N+1} & = & \infty & \end{array}, \tag{1.4}$$

where $K_n = -\ln(\text{BER}_0/a_n)$ [7, Eq. (5)].[7]

In [33, 34], the results in [7] and [32, Ch. 2] are extended to take both spatial diversity and feedback delay into account. Multiple antennas are introduced at the receiver, which effectively changes it from a SISO system to a SIMO system. MRC is used to combine the signals collected from H receiver antennas, and it is assumed that the MRC receiver operates on independent and identically distributed (i.i.d.) Rayleigh fading channels. A nonzero feedback delay τ is taken into account by assuming that the instantaneous SNR at time t has changed to γ_τ at time $t + \tau$. Since a change in the SNR reflects a change in the channel condition, there will be a mismatch between the reported CSI and the true state of the channel. This mismatch is modelled through the temporal correlation ρ between γ and γ_τ. In particular, the BER degradation due to a nonzero feedback delay is derived as a function of ρ.

In general, the average BER (averaged over all codes and SNRs) is obtained as the average number of bits in error, divided by the average number of bits transmitted [5]

$$\overline{\text{BER}} = \frac{\sum_{n=1}^N R_n \cdot \overline{\text{BER}}_n}{\sum_{n=1}^N R_n \cdot P_n}, \tag{1.5}$$

where $\overline{\text{BER}}_n$ is the average BER experienced when code n is applied. An expression for $\overline{\text{BER}}_n$ is derived by exploiting the approximation introduced in (1.3). However, a correction term for BER_n is introduced to account for the fact that (1.3) approaches a_n for low SNRs. Since a_n can be larger than one [7], the following expression is utilized in [33] and [34] to ensure that the exponential curve do not exceed 0.5:

$$\text{BER}_n = \begin{cases} a_n \cdot e^{-\frac{b_n \gamma}{M_n}} & \text{when } \gamma \geq \gamma_n^l \\ \frac{1}{2} & \text{when } \gamma < \gamma_n^l \end{cases} \tag{1.6}$$

The boundary $\gamma_n^l = \ln(2a_n)M_n/b_n$ is the smallest SNR such that the BER is no larger than 0.5 for either code.

---

[7] In [7], it is noted that it might not be obvious that $\gamma_n < \gamma_{n+1}$ for $n = 1, 2, \ldots, N$ since a_n and b_n vary with n. However, the monotonicity is attributed to the fact that, for a given BER, the minimum required SNR for $n+1$ is larger than the required SNR for code n when $M_{n+1} > M_n$. In practice, $0 < \text{BER}_0 < a_n$, in which case $K_n > 0$ and all the thresholds $\gamma_n > 0$.

At this point, it is noted that for two of the papers included in this thesis, the average BER performance is evaluated by utilizing the exponential BER approximation in (1.3) rather than the expression in (1.6), containing the correction term. However, according to [35], the average BER result is quite insensitive to overestimation for values above 10^{-1}. This is attributed to the fact that when the approximate BER curves for the individual codes are averaged, the values in the region above 10^{-1} are weighted by very low probabilities. Hence, it is then very unlikely that a code resulting in an instantaneous BER above 10^{-1} is selected. As a consequence, it is concluded that overestimation of the instantaneous BER at low SNRs has little or no influence on the average BER result.

In [32, Ch. 3] and [35], the results in [33, 34] are extended to include pilot-symbol assisted modulation (PSAM) [36], which is a technique where known symbols (pilot symbols) are multiplexed into the information data stream prior to transmission. Both the pilot symbols and the multiplexing scheme are known by the receiver and can be exploited for channel estimation and channel prediction. A baseband model of the rate-adaptive SIMO system is depicted in Figure 1.4, where channel estimation using PSAM is employed to achieve coherent detection of the data. In addition, PSAM is exploited for channel prediction to predict the future CSI as a remedy against the outdated CSI problem. Hence, instead of reporting a CSI based on the instantaneous SNR, a CSI based on a predicted SNR ahead in time is reported. Assuming that the prediction horizon equals the time delay on the feedback channel, the reported CSI will be more in accordance with the true state of the channel when it is used by the transmitter to select a code. Since the goal of the work in [32, Ch. 3] and [35] was to suggest bounds for the possible BER, ASE, and outage probability, a computationally intensive predictor, optimal in the *maximum a posteriori* (MAP) sense, is chosen. For details of MAP-optimal prediction with PSAM used in [32, 35], see [32, Sec. 3.5].

In Figure 1.4, the pilot symbols are extracted from the data symbols which are buffered before detection. Channel estimates at time instants other than pilot symbol instants are then obtained by using optimal noncausal Wiener interpolator filters provided on each antenna branch. Each of these filters operate on *maximum likelihood* (ML) estimates of the complex fading envelope at pilot symbol time instants. An estimate of this kind is the result of dividing a single observation of the noisy received signal by the known pilot symbol value [32, Eq. (3.8)]. In [37], it is noted that the interpolation coefficients can be kept constant over a whole pilot-period range L, but better channel estimates can be obtained if the interpolator coefficients are optimally updated for every received symbol. In this thesis,

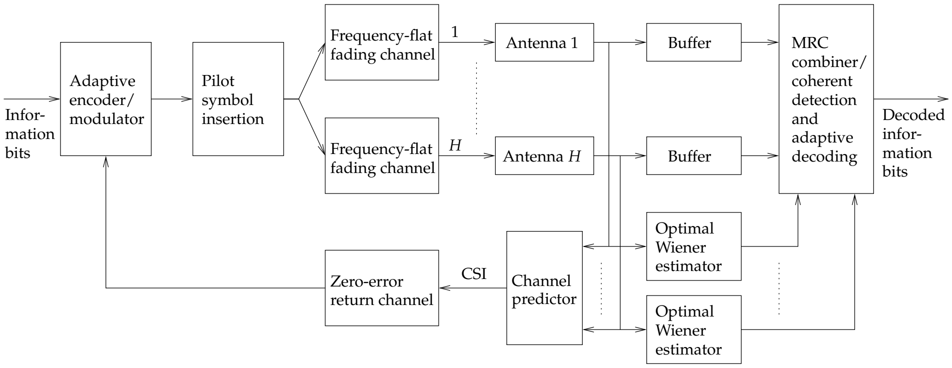
Information bits
Adaptive encoder/ modulator
Pilot symbol insertion
Frequency-flat fading channel
Frequency-flat fading channel
1
H
Antenna 1
Antenna H
Buffer
Buffer
MRC combiner/ coherent detection and adaptive decoding
Decoded information bits
Optimal Wiener estimator
Optimal Wiener estimator
Channel predictor
CSI
Zero-error return channel

FIGURE 1.4: ACM system with pilot-symbol-assisted channel estimation (for coherent detection) and prediction (for transmitter adaptation).

as in [32], it assumed that the fading process is constant between two successive pilot symbols, in which case constant interpolation coefficients can be used.

Channel estimation by using periodic insertion of pilot symbols can be viewed as sampling of a band-limited process. For a maximum Doppler frequency of f_D [Hz], the sampling frequency, f_{samp} [Hz], of the fading process must be equal to $f_{samp} \geq 2f_D$ in order to conform to the Nyquist sampling theorem [38]. As the time interval between two pilot symbols is equal to the sampling period, it can be written as $T_{samp} = 1/f_{samp} = LT_s$ [s]. Invoking the Nyquist condition, the pilot symbol spacing L must then satisfy the condition $L \leq 1/(2W)$, where $W = f_D T_s$ is the normalized Doppler spread (denoted as fading bandwidth in [39]).[8] According to [39, Eq. (21)], the estimation error of a single non-causal Wiener interpolator filter operating on a slowly varying Rayleigh fading channel is equal to

$$\sigma_e^2 = \frac{\Omega \cdot 2WLN_0}{P\Omega + 2WLN_0}, \tag{1.7}$$

where P [W] is the constant average transmit power, and N_0 is the variance of the complex AWGN. By once again applying the Nyquist condition and focusing on channel estimation on branch h, $2WL \leq 1$, which gives $\sigma_e^2 \leq \Omega/\overline{\gamma}_h$ [32, Eq. (3.7)], where $\overline{\gamma}_h = \frac{\Omega P}{N_0}$ is the average SNR received on branch h. Hence, it is noted that unless the average SNR is very low, it can be assumed that the estimation error in the receiver is negligible compared to the prediction error, i.e. signal detection can be assumed to be perfect.

---

[8] With the assumption of slow fading channels, $W \ll 0.5$.

Contributions of the included papers

This thesis consists of five papers, which are numbered with the capital letters A, B, C, D, and E. In the following, a summary of the included papers is presented.

Paper A

Bengt Holter and Geir E. Øien, "Performance analysis of a rate-adaptive dual-branch switched diversity system," *submitted to IEEE Transactions on Wireless Communications.*

In Paper A, the rate-adaptive SISO system in [7] is extended to a 1×2 SIMO system by using a dual-branch switched diversity combiner at the receiver. Similar extensions are reported in the literature, but they have so far only been focused on the MRC receiver [33, 34]. However, since MRC represents the diversity scheme with the highest complexity, other and less complex diversity schemes are often preferred in practice. A switched diversity combiner requires just a single receiver chain for its implementation, and only the channel state of the currently selected branch needs to be monitored. As such, it represents an attractive choice for a low complexity receiver.

The performance is evaluated for a system operating on identically distributed Nakagami-m fading channels with perfect channel knowledge at the receiver and instantaneous/time-delayed feedback of CSI. Both uncorrelated and correlated antenna branches are considered. The optimal switching threshold that maximizes the ASE is identified for the case of uncorrelated antenna branches.

It is concluded that in order to maximize the ASE for a given average SNR on the channels, the switching threshold must be identical to one of the predefined thresholds of the ACM scheme. In this case, the performance in terms of ASE and average BER is close to the performance obtained with both MRC and SC, but at a significantly lower complexity. The system benefits from second order diversity only as long as the switching threshold is in the vicinity of the average SNR on the channels. Hence, the performance approaches that of a single branch receiver if the switching threshold is either too low or too high compared to the average SNR. Similarly, the ASE approaches that of a single branch receiver when spatial correlation is introduced. The same effect is also visible for the average BER, but mainly at high SNR values. The impact of time-delayed feedback is presented for two isotropic scattering models: with and without a LOS component. In general, a normalized time delay of 10^{-2} is tolerated without a noticeable degradation in the average BER. A slight increase in tolerance is achieved by increasing the Nakagami-m fading parameter. In all cases, the time delay tolerance is smallest when there is a LOS component present, and the angle of arrival is in the same direction as the direction of motion. This causes the fastest decorrelation of the channel.

To our knowledge, a performance analysis of a switched diversity system utilizing an ACM scheme has not yet been reported in the literature. Paper A may be viewed as an attempt to fill this gap.

Paper B

Bengt Holter and Geir E. Øien, "Impact of spatial correlation on adaptive coded modulation performance in Rayleigh fading," *submitted to IEEE Transactions on Vehicular Technology.*

In Paper B, a performance analysis of an ACM scheme operating on a SIMO system with identically distributed and spatially correlated Rayleigh fading channels is presented. PSAM is employed for channel estimation and channel prediction, and MRC is used to combine signals from H receiver antennas. Rate adaptation is performed by providing the transmitter with CSI as *predicted* by the receiver. Numerical examples are provided for the case of Jakes fading spectrum and MAP-optimal predictor coefficients. As such, Paper B represents an extension of [32, Ch. 3] and [35] by taking spatial correlation into account.

In [32, Ch. 3] and [35], an important part of the analysis is based on the knowledge of the joint distribution of the true and predicted SNR, since the temporal correlation between these two entities is a vital parameter affecting the error performance. In particular, for uncorrelated Rayleigh fading channels, both the true and the predicted SNR are individually gamma distributed. As a result, the joint distribution is a bivariate gamma distribution. However, for spatially correlated channels, neither the true nor the predicted SNR will be gamma distributed. In fact, their true densities do not belong to any standard distribution, so the joint distribution needed to quantify the correlation is not known.

In Paper B, this is alleviated by approximating the true and the predicted SNR to be gamma distributed RVs with first and second order moments identical to those of the exact distribution. It is demonstrated that by using this approach, the same type of analysis as in [32, Ch. 3] and [35] may be pursued with good accuracy for both low and medium SNR values. The SNR range must however be upper limited, since the gamma distribution does not contribute to realize the true slope (diversity order) or coding gain of the error rate curve at high SNR. The valid SNR range is determined by comparing results for the error rate curves obtained with the true (non-gamma) PDF and the approximate (gamma) PDF under idealized assumptions (perfect channel knowledge, perfect CSI, and zero delay on the feedback channel). It is argued that the imposed SNR upper limit does not represent a major limitation of the work, since at high SNR, only the largest available signal constellation will be used. In this case, the system resembles a fixed rate system, for which the effects of channel correlation is well known and well documented in the literature (see for instance [8, Sec. 9.6]).

Spatial/temporal separability is assumed, i.e. the normalized cross correlation between complex fading envelopes on different branches is represented as a product of the individual spatial and temporal correlations. Under this assumption, the temporal correlation coefficient between the true and predicted SNR is shown to be identical to the one obtained for uncorrelated channels in [32, Ch. 3] and [35]. According to [40], spatial/temporal separability of the cross correlation function is adequate for gauging average system behavior.

For a given set of SNR thresholds/fading bins, it is concluded that spatial correlation has a significant impact on the BER performance, by reducing "the acceptable BER" region, where the system operates reliably with respect to average SNR and permitted time delay on the feedback channel. However, when the system operates below the target BER (acceptable region), the performance degradation in terms of ASE caused by spatial correlation is not large.

Paper C

Bengt Holter, Geir E. Øien, Kjell J. Hole, and Henrik Holm, "Limitations in spectral efficiency of a rate-adaptive MIMO system utilizing pilot-aided channel prediction," *in Proc. Vehicular Technology Conference*, Jeju, Korea, April 2003.

In Paper C, the rate-adaptive SIMO system in [32, Ch. 3] and [35] is extended to a MIMO system. In particular, a MIMO *diversity* system is considered, in which case orthogonal STBC is used at the transmitter to maximize the diversity order [14]. For such a MIMO system, performance merits can be obtained by following the same analysis approach as in [32, Ch. 3] and [35]. PSAM is used for channel estimation and channel prediction, but since multiple transmit antennas are introduced, the channel estimation task is different from a SIMO system. Identical pilot symbols can not be transmitted simultaneously from all the transmit antennas, since the received signal on each branch will then be a combination of channel responses.

Hence, in order to estimate all the channels, the pilot symbol can only be transmitted by a single antenna at a time [12, Sec. VB].[9] As a result, sampling of the channel with PSAM is performed by letting the pilot symbol alternate between the transmit antennas.

An obvious disadvantage of this channel estimation technique is that more time is spent on transmitting pilot-symbols, which contributes to reduce the ASE compared to a SIMO system with the same set of available codes, the same SNR thresholds, and the same pilot symbol period. Another factor contributing to reduce the ASE is that the code rate of an orthogonal STBC based on a complex signal constellation is less than one when more than two transmit antennas are employed [13].

Based on these facts, it is concluded that the ASE of the considered MIMO diversity system is upper bounded, for a given pilot period L, by the ASE of the SIMO system in [32, Ch. 3] and [35]. Apart from that, it is observed that the acceptable BER region is very similar for SIMO and MIMO systems having the same diversity order.

Unfortunately, the original published version of Paper C contains some misprints and some minor errors in the numerical results. These have been corrected in Paper C. For the sake of clarity, a list of the corrected misprints and some comments to Paper C are provided:

- All the performance results in Paper C are *numerical* results. Hence, the word *simulation*, which is used several times in the original paper [41], is misleading and have been replaced by the word *numerical* in Paper C.
- In [41], the pilot symbol spacing on a single branch L_b is written as $L_b = (1/R_s)m \cdot n_T + n_T$. This is not wrong, but it is applicable only to the orthogonal designs G_2, G_4, and H_3. In Paper C, it has been replaced by the more general expression $L_b = (1/R_s)m \cdot K + n_T$
- The numerical results depicted in Fig. 4 and 5 in [41] are obtained by using the pilot symbol spacing L on the input of the space-time encoder. However, prior to transmission, the distance between pilot-symbols is increased to L_b on each branch. Hence, instead of $L = 7$, the results should have been derived with $L_b = 8$ and $L_b = 11$, respectively. In Paper C, these results have been corrected. Since the changes from L to L_b in these cases are very small, the new results are not far from the original ones in [41].

---

[9] In [12, Sec. VB], it is argued that simultaneous transmission of pilot-symbols may be used in a MISO system if orthogonal pilot symbols are employed.

- In [41, Fig. 6], the relative differences in ASE between a 1×4, 2×2, and a 3×3 system are depicted for various pilot symbol spacings L at the input of the space-time encoder. For the 2×2 system, the STBC G_2 is employed, while for the 3×3 system, the STBC H_3 is employed. This information has been added to the figure caption of Figure C.6 in Paper C. The ASE is almost independent of the feedback delay when the normalized delay is in the region $0 - 0.25$, but due to space limitations, this is not reflected in [41]. As a result, the ASE obtained for a normalized time delay of 0.25 (depicted in Figure C.6), is almost identical to the result obtained with zero time delay. However, it is emphasized here that the ASE results depicted in Figure C.6 are meaningful only for the CSNR/delay combinations where the target BER constraint is fulfilled in the Figures C.3, C.4, and C.5.
- In the third paragraph of Section 3 (SIMO channel model), there is a misprint. The overall expected CSNR has been corrected from γ to $\overline{\gamma}$ in Paper C.
- In the numerical results, the spectral efficiencies $\{R_n\}_{n=1}^{N}$ are derived for $G = 2$ (as employed in [7, 32]). The use of $G = 2$ is not explicitly mentioned in [41], but included in Paper C.
- In [41, Eq. (5)], a subindex n is missing. In Paper C, it has been corrected to $\text{BER}_n \approx a_n \cdot e^{-\frac{b_n \gamma}{M_n}}$.
- In [41, Eq. (6)], there are two misprints. In Paper C, the following corrections have been made. Firstly, the sign $\cong$ is changed into an equality. Secondly, the condition $\gamma \leq \gamma_n^l$ is changed to $\gamma < \gamma_n^l$.
- For consistency, the notation of the normalized complementary incomplete gamma function has been changed from $Q(x, y)$ to $\overline{\Gamma}(x, y)$ to avoid confusion with the generalized first order Marcum-Q function.
- Finally, it is noted that since the pilot symbols are transmitted on one branch at a time, it is assumed that each such symbol is transmitted with the total available power.

Paper D

Bengt Holter and Geir E. Øien, "On the amount of fading in MIMO diversity systems," *accepted for publication in IEEE Transactions on Wireless Communications.*

For wireless systems using spatial diversity combining techniques to reduce the impact of fading, it is of interest to employ measures which can capture and quantify the performance improvement related to a reduced fading level. The average error rate is typically used, in which case a potential improvement is quantified through a slope change and/or a horizontal shift of the error rate curve relative to a benchmark curve at high SNR. However, the exact error rate may in some cases be difficult to evaluate analytically, since it requires statistical averaging of the conditional error rate with a particular fading distribution. A more simple yet effective way of quantifying the severity of fading can be obtained by using a measure directly related to the moments of the fading distribution itself. One such measure is the *amount of fading* (AF) [42], defined as the variance of the squared fading amplitude divided by the squared mean. As such, the AF is related to the kurtosis, which is a measure of the peakedness of a distribution. The higher the kurtosis, the lower the concentration of the density function around its mean. It takes its minimum value for deterministic variables. In particular, the AF is equal to the kurtosis minus 1 [43].

In [42], the AF was introduced to quantify the severity of fading experienced at the output of a SISO system when different channel fading models were applied. In particular, for the Nakagami-m fading model, $\text{AF} = 1/m$ for $m \geq 1/2$. Hence, as the Nakagami-m fading parameter increases, the AF decreases. In the limit, as $m \to \infty$, the Nakagami-m fading channel converges to a nonfading AWGN channel with $\text{AF} = 0$. In [8, Ch. 2], expressions for the AF in a SISO system are presented for a wide variety of fading distributions.

In contrast to a SISO system, the AF is in Paper D employed to quantify the degree of fading experienced at the output of a MIMO diversity system. A closed-form expression is presented when the system operates on identically distributed spatially correlated Nakagami-m fading channels. With the assumption of independent correlation properties at the transmitter and the receiver, the AF is presented for identically distributed Rayleigh fading channels and different types of correlation models. By capitalizing on recent results in [44], it is shown that for a constant correlation model, the average symbol error probability at the output of a MIMO diversity system at high SNR may be expressed in terms of the AF.

Paper E

Bengt Holter, Mohamed-Slim Alouini, Geir E. Øien and Hong-Chuan Yang, "Multiuser switched diversity transmission," *in Proc. Vehicular Technology Conference*, Los Angeles, USA, September 2004.

In a multiuser system, multiuser diversity may be exploited to maximize the average system throughput by always serving the user with the best channel. A traditional way of performing this task in a time-division multiplexed system is to let the BS probe all the users and select the user which reports the best channel quality at any given time-slot. This method yields the best ASE for a given target BER, but it comes at the expense of a high and deterministic *feedback load* (number of users the BS has to probe before one user is given access to the channel).

The key observation utilized in Paper E is that algorithms originally devised to select between antennas in a spatial diversity system may also be applied as multiuser access schemes. The reasoning behind this argument is that a system exploiting multiuser diversity may be looked upon as a traditional spatial diversity system, in which the antennas of the spatial diversity combiner (acting as a BS) have been replaced by users, each having a single antenna. As a result, a multiuser access scheme based on always serving the user with the strongest channel is equivalent to SC. The feedback load of SC is deterministic and equal to the total number of users connected to the BS. In an attempt to simplify the selection procedure and reduce the feedback load, a set of *switched* multiuser access schemes are proposed. The new access schemes are all based on *switched* diversity algorithms originally devised to select between antennas in a spatial diversity system, and the basic principle is to look for an *acceptable* user rather looking for the ultimate best user. A user qualifies as an acceptable user and is selected by the BS when the reported channel quality is above a predefined switching threshold.

The ACM scheme in [7] is utilized on each selected link to ensure a high ASE of the system. For simplicity, i.i.d. Rayleigh fading channels across the different users are assumed, and the individual users and the BS are all equipped with just a single antenna. Perfect channel knowledge is assumed at both the BS and the users.

Numerical results quantifying the trade-off between ASE and *average* feedback load (AFL) are presented, using the access scheme based on SC as a benchmark. It is concluded that the proposed access schemes can contribute to reduce the AFL significantly without experiencing a big performance loss. In addition, it is argued that the switched access schemes are quite attractive also from a fairness perspective.

For Paper E, the following comments are in order:

- one may argue that with a fixed guard time, the benefit of using a switched access scheme is lost, since the BS or the selected terminal anyway has to wait until the guard period is finished before transmission of data can commence. As a result, since the entire guard time period is used, all the users could have been asked for their channel status. However, with the proposed switched access schemes, all the terminals may operate in a sleep mode or power saving mode as long as they do not transmit data or respond to a call from the BS. This lead to significant power savings compared to the benchmark scheme where each terminal must power up and report their channel status in every time slot. In addition, less traffic is generated in the system, since on average, just a small percentage of the users need to report their channel status for each time slot. Both these gains come at the expense of a small reduction in ASE.

Main contributions of the thesis

As a summary, this section states the main contributions of the thesis.

- A performance analysis of an ACM scheme in a SIMO system using a dual-branch switched diversity combiner at the receiver is presented. To our knowledge, this has not yet been reported in the literature.
- A performance analysis of an ACM scheme in a SIMO system with an MRC receiver operating on identically distributed but *spatially correlated* Rayleigh fading channels is presented.
- A performance analysis of an ACM scheme in a MIMO diversity system is presented. The reduction in ASE incurred by using ACM and PSAM in such a system has been quantified.
- The degree of fading mitigating at the output of a MIMO diversity system has been quantified by using a measure called *amount of fading*. In particular, a closed-form expression for the amount of fading is derived for a MIMO diversity system operating on identically distributed and spatially correlated Nakagami-m fading channels. For independent correlation properties at the transmitter and receiver, amount of fading expressions are derived for different antenna correlation models.
- By capitalizing on results in [44], it is shown that for a constant correlation model, the average symbol error probability at the output of a MIMO diversity system at high SNR may be expressed in terms of the amount of fading.

- Spatial diversity algorithms originally devised to select between antennas have been utilized as multiuser access schemes in a multiuser system. The proposed access schemes can contribute to reduce the average feedback load significantly compared to systems relying on feedback from all the users, without experiencing a big performance loss.
- An eigenfilter approach to obtain the optimal weights of an MRC receiver is presented.

Suggestions for further research

In Paper B and C, PSAM is utilized for channel estimation and channel prediction. However, the pilot symbol spacing L is fixed, and the pilot symbols are transmitted with the same power as the data symbols. A natural extension is to include adaptive PSAM, where both L and the power ratio between pilots and data symbols are adaptively optimized to maximize the ASE subject to the constraint $\text{BER} \leq \text{BER}_0$. In addition, imperfect CSI at both the receiver and transmitter should be taken into account. Current research within this area is reported in [45–48].

In Paper C, the focus is on reliable transmission by exploiting multiple antennas at both the transmitter and the receiver to maximize the overall diversity order. A natural extension is to investigate the performance of ACM in a spatial multiplexing system. In addition, only narrowband flat-fading channels have been considered. Orthogonal frequency division multiplexing (OFDM) could be introduced to extend the methods of ACM to wideband transmission. In particular, the combination of OFDM and MIMO is an interesting topic for further research. OFDM can transform a frequency-selective MIMO channel into a set of parallel frequency-flat MIMO channels, as long as the length of the channel impulse response is smaller than or equal to the cyclic prefix (CP) length. As such, narrowband spatial multiplexing receivers can be applied on a tone-by-tone basis [49]. STBC can also be combined with OFDM transmission, achieving spatial diversity gains over frequency-selective fading channels. Then, STBC is applied on adjacent blocks of data symbols (OFDM symbols) rather than on individual data symbols.

Finally, an interesting topic for further research within the context of adaptive MIMO systems is to apply reconfigurable antenna arrays. Recall that in multiple-antenna channels, the channel capacity grows linearly with the number of spatial degrees of freedom. However, as noted in [50], packing more antennas in a given area will just make the fading correlated, so increasing the number of antennas within a confined space cannot increase the capacity indefinitely. With the advent of RF MEMS[10] [51], a class of new components which display superior high-frequency performance relative to conventional semiconductor devices can be used to implement reconfigurable antenna arrays [52]. A reconfigurable antenna array can adapt its geometrical size by changing the antenna element spacing using MEMS switches [53]. As such, the number of spatial degrees of freedom can be adapted to the current needs. For instance, beamforming requires closely spaced antennas to avoid grating lobes, while spatial diversity techniques for diversity maximization will perform well if the antennas are sufficiently separated to ensure low correlation. Hence, a reconfigurable antenna array represents additional degrees of freedom in an adaptive MIMO system.

---

[10] Micro-Electro-Mechanical Systems

References

[1] J. F. Hayes, "Adaptive feedback communications," *IEEE Transactions on Communication Technology*, vol. COM-16, pp. 29–34, February 1968.

[2] J. K. Cavers, "Variable-rate transmission for Rayleigh fading channels," *IEEE Transactions on Communications*, vol. COM-20, no. 1, pp. 15–22, February 1972.

[3] W. T. Webb and R. Steele, "Variable-rate QAM for mobile radio," *IEEE Transactions on Communications*, vol. 43, no. 7, pp. 2223–2230, July 1995.

[4] A. J. Goldsmith and S. -G. Chua, "Variable-rate variable-power M-QAM for fading channels," *IEEE Transactions on Communications*, vol. 45, no. 10, pp. 1218–1230, October 1997.

[5] M. -S. Alouini and A. J. Goldsmith, "Adaptive modulation over Nakagami fading channels," *Wireless Personal Communications*, vol. 13, pp. 119–143, May 2000.

[6] A. J. Goldsmith and S. -G. Chua, "Adaptive coded modulation for flat fading channels," *IEEE Transactions on Communications*, vol. 46, no. 5, pp. 595–602, May 1998.

[7] K. J. Hole, H. Holm, and G. E. Øien, "Adaptive multidimensional coded modulation on flat fading channels," *IEEE Journal on Selected Areas in Communications*, vol. 18, no. 7, pp. 1153–1158, July 2000.

[8] M. K. Simon and M. -S. Alouini, *Digital Communications over Fading Channels: A Unified Approach to Performance Analysis*. New York: Wiley, 2000.

[9] G. L. Stüber, *Principles of Mobile Communications*. Second edition, Kluwer Academic Publishers, 2001.

[10] M. Nakagami, “The *m*-distribution, a general formula of intensity distribution of rapid fading,” *Statistical Methods in Radio Wave Propagation*, pp. 3–36, June 1960.

[11] I. S. Gradshteyn and I. M. Ryzhik, *Table of Integrals, Series, and Products*. 5th ed., San Diego, CA: Academic Press, 1994.

[12] S. M. Alamouti, “A simple transmit diversity technique for wireless communications,” *IEEE Journal on Selected Areas in Communications*, vol. 16, no. 8, pp. 1451–1458, October 1998.

[13] V. Tarokh, H. Jafarkhani, and A. R. Calderbank, “Space-time block codes from orthogonal designs,” *IEEE Transactions on Information Theory*, vol. 45, no. 5, pp. 1456–1467, July 1999.

[14] R. W. Heath, “Space-time signaling in multi-antenna systems,” Ph.D. dissertation, Stanford University, November 2001.

[15] G. J. Foschini and M. J. Gans, “On limits of wireless communications in a fading environment when using multiple antennas,” *Wireless Personal Communications*, vol. 6, pp. 311–335, March 1998.

[16] B. Holter, “On the capacity of the MIMO channel - a tutorial introduction.” *in Proc. IEEE Norwegian Symposium on Signal Processing*, pp. 167–172, October 2001.

[17] D. Gesbert, M. Shafi, D. S. Shiu, P. J. Smith, and A. Naguib, “From theory to practice: an overview of MIMO space-time coded wireless systems,” *IEEE Journal on Selected Areas in Communications*, vol. 21, no. 3, pp. 281–302, April 2003.

[18] S. Sandhu and A. Paulraj, “Space-time block codes: a capacity perspective,” *IEEE Communications Letters*, vol. 4, no. 12, pp. 384–386, December 2000.

[19] D. G. Brennan, “Linear diversity combining techniques,” *in Proc. IRE*, vol. 47, pp. 1075–1102, 1959.

[20] S. Haykin, *Adaptive Filter Theory*. Prentice-Hall, Inc., 2002.

[21] B. Holter and G. E. Øien, “The optimal weights of a maximum ratio combiner using an eigenfilter approach,” *in Proc. 5th IEEE Nordic Signal Processing Symposium*, October 2002.

[22] R. Knopp and P. A. Humblet, "Information capacity and power control in single cell multiuser communications," *in Proc. IEEE International Conference on Communications*, vol. 1, pp. 331–335, June 1995.

[23] P. Viswanath, D. N. C. Tse, and R. Laroia, "Opportunistic beamforming using dumb antennas," *IEEE Transactions on Information Theory*, vol. 48, no. 6, pp. 1277–1294, June 2002.

[24] D. N. C. Tse and S. V. Hanly, "Multiaccess fading channels - part I: Polymatroid structure, optimal resource allocation and throughput capacities," *IEEE Transactions on Information Theory*, vol. 44, no. 7, pp. 2796–2815, November 1998.

[25] L. Li and A. J. Goldsmith, "Capacity and optimal resource allocation for fading broadcast channels - part I: Ergodic capacity," *IEEE Transactions on Information Theory*, vol. 47, no. 3, pp. 1083–1102, March 2001.

[26] D. Gesbert and M. -S. Alouini, "How much feedback is multi-user diversity really worth ?" *in Proc. IEEE International Conference on Communications*, pp. 234–238, June 2004.

[27] L. Yang, M. -S. Alouini, and D. Gesbert, "Further results on selective multi-user diversity," *in Proc. Seventh ACM/IEEE International Symposium on Modeling, Analysis and Simulation of Wireless and Mobile Systems*, October 2004.

[28] H. Koubaa, V. Hassel, and G. E. Øien, "Multiuser diversity gain enhancement by guard time reduction," *Temporary Document TD(05)-038, 12th Management Committee Meeting, COST Action 273 Towards Mobile Multimedia Broadband Networks*, January 2005.

[29] V. Hassel, M. -S. Alouini, D. Gesbert, and G. E. Øien, "Minimizing feedback load for nested scheduling algorithms," *accepted for publication in Proc. IEEE Vehicular Technology Conference*, May 2005.

[30] R. Gozali, R. M. Buehrer, and B. D. Woerner, "The impact of multiuser diversity on space-time block coding," *IEEE Communications Letters*, vol. 7, no. 5, pp. 213–215, May 2003.

[31] E. G. Larsson, "On the combination of spatial diversity and multiuser diversity," *IEEE Communications Letters*, vol. 8, no. 8, pp. 517–519, August 2004.

[32] H. Holm, "Adaptive coded modulation and channel estimation tools for flat fading channels," Ph.D. dissertation, The Norwegian University of Science and Technology, April 2002 (available at: http://www.tele.ntnu.no/projects/beats/theses.htm).

[33] K. J. Hole, H. Holm, and G. E. Øien, "Analysis of adaptive coded modulation with antenna diversity and feedback delay," *in Proc. IST Mobile Communications Summit*, pp. 865–870, September 2001.

[34] ——, "Performance analysis of adaptive coded modulation with antenna diversity and feedback delay," *Telektronikk*, vol. 98, no. 1, pp. 106–113, 2002.

[35] G. E. Øien, H. Holm, and K. J. Hole, "Impact of channel prediction on adaptive coded modulation performance in Rayleigh fading," *IEEE Transactions on Vehicular Technology*, vol. 53, no. 3, pp. 758–769, May 2004.

[36] J. K. Cavers, "An analysis of pilot symbol assisted modulation for Rayleigh fading channels," *IEEE Transactions on Vehicular Technology*, vol. 40, no. 4, pp. 686–693, November 1991.

[37] J. M. Torrance and L. Hanzo, "Comparative study of pilot symbol assisted modulation schemes," *in Proc. IEE Sixth International Conference on Radio Receivers and Associated Systems*, no. 415, pp. 36–41, September 1995.

[38] S. Haykin, *Communication Systems*. John Wiley & Sons, Inc., 1994.

[39] G. E. Øien and K. J. Hole, "Maximum average spectral efficiency of slowly varying Rayleigh fading channels with pilot-symbol-assisted channel estimation," *in Proc. European Personal Mobile Communications Conference*, February 2001.

[40] P. J. Smith and M. Shafi, "The impact of complexity in MIMO channel models," *in Proc. IEEE International Conference on Communications*, vol. 5, pp. 2924–2928, June 2004.

[41] B. Holter, G. E. Øien, K. J. Hole, and H. Holm, "Limitations in spectral efficiency of a rate-adaptive MIMO system utilizing pilot-aided channel prediction," *in Proc. Vehicular Technology Conference*, vol. 1, pp. 282–286, April 2003.

[42] U. Charash, “Reception through Nakagami fading multipath channels with random delays,” *IEEE Transactions on Communications*, vol. COM-27, no. 4, pp. 657–670, April 1979.

[43] S. Verdú, “Spectral efficiency in the wideband regime,” *IEEE Transactions on Information Theory*, vol. 48, no. 6, pp. 1319–1343, June 2002.

[44] Z. Wang and G. B. Giannakis, “A simple and general parameterization quantifying performance in fading channels,” *IEEE Transactions on Communications*, vol. 51, no. 8, pp. 1389–1398, August 2003.

[45] D. V. Duong and G. E. Øien, “Adaptive trellis-coded modulation with imperfect channel state information at the receiver and transmitter,” *in Proc. Nordic Radio Symposium*, August 2004.

[46] D. V. Duong, G. E. Øien, and K. J. Hole, “Adaptive coded modulation with receive antenna diversity and imperfect channel knowledge at receiver and transmitter,” *Temporary Document TD(05)-009, 12th Management Committee Meeting, COST Action 273 Towards Mobile Multimedia Broadband Networks*, January 2005.

[47] D. V. Duong, B. Holter, and G. E. Øien, “Optimal pilot spacing and power in rate-adaptive MIMO diversity systems with imperfect transmitter CSI,” *submitted to the VI IEEE Workshop on Signal Processing Advances in Wireless Communications*, 2005.

[48] X. Cai and G. B. Giannakis, “Adaptive PSAM accounting for channel estimation and prediction errors,” *IEEE Transactions on Wireless Communications*, vol. 4, no. 1, pp. 246–256, January 2005.

[49] H. Bölcskei, D. Gesbert, and A. J. Paulraj, “On the capacity of OFDM-based spatial multiplexing systems,” *IEEE Transactions on Communications*, vol. 50, no. 2, pp. 225–234, February 2002.

[50] A. S. Y. Poon, R. W. Brodersen, and D. N. C. Tse, “Degrees of freedom in multiple-antenna channels: A signal space approach,” *IEEE Transactions on Information Theory*, vol. 51, no. 2, pp. 523–536, February 2005.

[51] M. Sadiku, “MEMS,” *IEEE Potentials*, vol. 21, no. 1, pp. 4–5, February 2002.

[52] B. A. Centiner, H. Jafarkhani, J. -Y. Qian, H. J. Yoo, A. Grau, and F. D. Flaviis, “Multifunctional reconfigurable MEMS integrated anten-

nas for adaptive MIMO systems," *IEEE Communications Magazine*, vol. 42, no. 12, pp. 62–70, December 2004.

[53] E. R. Brown, "RF-MEMS switches for reconfigurable integrated circuits," *IEEE Transactions on Microwave Theory*, vol. 46, no. 11, pp. 1868–1880, November 1998.

Part II

Included papers

Papers A,B,C,D and E are not included due to copyright.

Part III

Appendices

Appendix 1

The generalized Marcum Q-function

The generalized Marcum Q-function as defined by Nuttall is equal to [1]

$$Q_m(a,b) = \frac{1}{a^{m-1}} \int_b^\infty x^m e^{-\frac{(x^2+a^2)}{2}} I_{m-1}(ax)dx, \tag{1.1}$$

where a and b are nonnegative real numbers, and m is a nonnegative integer. The function $I_{m-1}(\cdot)$ is the modified Bessel function of the first kind of order $m-1$ [2]. In [3, Ch. 11.4], Temme uses a slightly different definition, written as

$$\widetilde{Q}_m(\alpha,\beta) = \int_\beta^\infty \left(\frac{x}{\alpha}\right)^{\frac{1}{2}(m-1)} e^{-x-\alpha} I_{m-1}(2\sqrt{\alpha x})dx. \tag{1.2}$$

The conversion between these two definitions is defined

$$Q_m(a,b) = \widetilde{Q}_m\left(\frac{a^2}{2}, \frac{b^2}{2}\right). \tag{1.3}$$

Proof: By substituting $z = x^2/2$ and $c = a^2/2$ in (1.1), and defining $d = b^2/2$, the following chain of equalities are obtained

$$\begin{aligned} Q_m(a,b) &= \frac{1}{(\sqrt{2c})^{m-1}} \int_{b^2/2}^\infty (\sqrt{2z})^m e^{-z-c} I_{m-1}\left(2\sqrt{cz}\right) \frac{1}{\sqrt{2z}} dz \\ &= \int_d^\infty \left(\frac{z}{c}\right)^{\frac{1}{2}(m-1)} e^{-z-c} I_{m-1}\left(2\sqrt{cz}\right) dz = \widetilde{Q}_m(c,d) = \widetilde{Q}_m\left(\frac{a^2}{2}, \frac{b^2}{2}\right). \end{aligned}$$

References

[1] A. H. Nuttall, "Some integrals involving the Q_M function," *IEEE Transactions on Information Theory*, vol. IT-21, no. 1, pp. 95–96, January 1975.

[2] I. S. Gradshteyn and I. M. Ryzhik, *Table of Integrals, Series, and Products*. 5th ed., San Diego, CA: Academic Press, 1994.

[3] N. M. Temme, *Special Functions: An Introduction to Classical Functions of Mathematical Physics*. New York: Wiley, 1996.

Appendix 2

Useful integration rules

$$\begin{aligned}\int_0^y e^{-au} Q_1\left(\alpha\sqrt{u}, \beta\right) du &= \frac{1}{a}\left[e^{-\frac{a\beta^2}{2a+\alpha^2}} Q_1\left(\sqrt{y}\sqrt{2a+\alpha^2}, \frac{\alpha\beta}{\sqrt{2a+\alpha^2}}\right)\right. \\ &- \left. e^{-ay} Q_1(\alpha\sqrt{y}, \beta)\right] \qquad (2.1)\end{aligned}$$

Proof: Substitute $x^2 = u$ in [1, Eq. (B.19)] and the proof follows easily. ☐

$$\begin{aligned}\int_x^y e^{-au} Q_1\left(\alpha\sqrt{u}, \beta\right) du &= \frac{1}{a}\left(e^{-ax} Q_1\left(\alpha\sqrt{x}, \beta\right) - e^{-ay} Q_1\left(\alpha\sqrt{y}, \beta\right)\right) \\ &+ \frac{1}{a} e^{-\frac{a\beta^2}{2a+\alpha^2}}\left[Q_1\left(\sqrt{y}\sqrt{2a+\alpha^2}, \frac{\alpha\beta}{\sqrt{2a+\alpha^2}}\right)\right. \\ &- \left. Q_1\left(\sqrt{x}\sqrt{2a+\alpha^2}, \frac{\alpha\beta}{\sqrt{2a+\alpha^2}}\right)\right] \qquad (2.2)\end{aligned}$$

Proof: Define the finite range integral as the difference between two integrals defined in (2.1) and the proof follows easily. ☐

$$\begin{aligned}&\int_0^\infty u^{\frac{m-1}{2}} e^{-\beta u} I_{m-1}(c\sqrt{u}) Q_m(a\sqrt{u}, b) du = \\ &\quad \frac{2}{c}\left(\frac{c}{2\beta}\right)^m e^{\frac{c^2}{4\beta}} Q_m\left(\frac{ac}{\sqrt{2\beta}\sqrt{2\beta+a^2}}, \frac{b\sqrt{2\beta}}{\sqrt{2\beta+a^2}}\right) \qquad (2.3)\end{aligned}$$

Proof: Substitute $x^2 = u$ in [2, Eq. (15)] and the proof follows easily. ☐

$$\begin{aligned}\int_x^y u^{m-1}e^{-cu}Q_m(a\sqrt{u},b)du &= \sum_{i=0}^{\infty}\frac{a^{2i}}{2^i i!}\frac{\Gamma(m+i,b^2/2)}{(c+a^2/2)^{m+i}} \\ &\times \left[\overline{\Gamma}(m+i,(c+a^2/2)x)\right. \\ &- \left.\overline{\Gamma}(m+i,(c+a^2/2)y)\right] \qquad (2.4)\end{aligned}$$

Proof: Employ (1.3) in Appendix 1 to the generalized Marcum-Q function and then use the infinite series representation of the Marcum-Q function as defined by Temme [3, Eq. (11.61)] and solve the new integral by employing [4, Eq. (C.1)]. ☐

For integer α and $\beta u \geq 0$:

$$\int_x^y u^{m-1}e^{-au}\overline{\Gamma}(\alpha,\beta u)du = \sum_{n=0}^{\alpha-1}\frac{\beta^n}{n!}\left[\frac{\Gamma(m+n,x(a+\beta))-\Gamma(m+n,y(a+\beta))}{(a+\beta)^{m+n}}\right] \qquad (2.5)$$

Proof: Substitute $\overline{\Gamma}(\alpha,\beta u) = e^{-\beta u}\sum_{n=0}^{\alpha-1}\frac{(\beta u)^n}{n!}$ [3, Eq. (11.6)] and the proof follows easily. ☐

References

[1] M. K. Simon, *Probability distributions involving gaussian random variables*. Kluwer Academic Publishers, 2002.

[2] A. H. Nuttall, "Some integrals involving the Q_M function," *IEEE Transactions on Information Theory*, vol. IT-21, no. 1, pp. 95–96, January 1975.

[3] N. M. Temme, *Special Functions: An Introduction to Classical Functions of Mathematical Physics*. New York: Wiley, 1996.

[4] H. Holm, "Adaptive coded modulation and channel estimation tools for flat fading channels," Ph.D. dissertation, The Norwegian University of Science and Technology, April 2002 (available at: http://www.tele.ntnu.no/projects/beats/theses.htm).

Appendix 3

Detailed derivation of the expression in (B.35)

Following the steps outlined in [1, Appendix B] for the term $\mathcal{E}\{\hat{\alpha}_h^2\alpha_i^2\}$:

$$\begin{aligned}
\mathcal{E}\{\hat{\alpha}_h^2\alpha_i^2\} &= \mathcal{E}\left[|\mathbf{f}_j^{\mathrm{H}}\tilde{\mathbf{z}}_h|^2 \cdot |z_i(n+j)|^2\right] \\
&= \mathbf{f}_j^{\mathrm{H}}\mathcal{E}\left[(\mathbf{z}_h + (1/a_p)\mathbf{n})(\mathbf{z}_h^{\mathrm{H}} + (1/a_p)\mathbf{n}^{\mathrm{H}})\right. \\
&\times \left.|z_i(n+j)|^2\right]\mathbf{f}_j. \qquad (3.1)
\end{aligned}$$

Since noise and fading are statistically independent and both zero-mean,

$$\begin{aligned}
\mathcal{E}\{\hat{\alpha}_h^2\alpha_i^2\} &= \mathbf{f}_j^{\mathrm{H}}\mathcal{E}\left[\mathbf{z}_h\mathbf{z}_h^{\mathrm{H}} \cdot |z_i(n+j)|^2 + (1/a_p^2)\mathbf{n}\mathbf{n}^{\mathrm{H}} \cdot |z_i(n+j)|^2\right]\mathbf{f}_j \\
&= \mathbf{f}_j^{\mathrm{H}}\mathcal{E}\left[\mathbf{z}_h\mathbf{z}_h^{\mathrm{H}} \cdot |z_i(n+j)|^2\right]\mathbf{f}_j + \Omega\frac{N_0B}{a_p^2}\|\mathbf{f}_j\|^2. \qquad (3.2)
\end{aligned}$$

Introducing $\mathbf{z}_{r,h} = \Re(\mathbf{z})_h$ and $\mathbf{z}_{i,h} = \Im(\mathbf{z})_h$ (and similarly for the complex scalar $z_i(n+j)$), where $\Re(\cdot)$ and $\Im(\cdot)$ denotes the real and imaginary parts of a complex symbol, respectively:

$$\begin{aligned}
\mathcal{E}\{\hat{\alpha}_h^2\alpha_i^2\} &= \mathbf{f}_j^{\mathrm{H}}\mathcal{E}\left[(\mathbf{z}_{r,h}\mathbf{z}_{r,h}^{\mathrm{T}} + \jmath\mathbf{z}_{i,h}\mathbf{z}_{i,h}^{\mathrm{T}}) \cdot (z_{r,i}^2(n+j) + z_{i,i}^2(n+j))\right]\mathbf{f}_j \\
&+ \frac{\Omega^2}{\overline{\gamma}_i}\|\mathbf{f}_j\|^2, \qquad (3.3)
\end{aligned}$$

which is identical to

$$\begin{aligned}\mathcal{E}\{\hat{\alpha}_h^2\alpha_i^2\} &= \mathbf{f}_j^{\mathrm{H}}\mathcal{E}\left[z_{r,i}(n+j)z_{r,i}(n+j)\mathbf{z}_{r,h}\mathbf{z}_{r,h}^{\mathrm{T}}\right]\mathbf{f}_j \\ &+ \mathbf{f}_j^{\mathrm{H}}\mathcal{E}\left[z_{i,i}(n+j)z_{i,i}(n+j)\mathbf{z}_{r,h}\mathbf{z}_{r,h}^{\mathrm{T}}\right]\mathbf{f}_j \\ &+ \mathbf{f}_j^{\mathrm{H}}\mathcal{E}\left[z_{r,i}(n+j)z_{r,i}(n+j)\mathbf{z}_{i,h}\mathbf{z}_{i,h}^{\mathrm{T}}\right]\mathbf{f}_j \\ &+ \mathbf{f}_j^{\mathrm{H}}\mathcal{E}\left[z_{i,i}(n+j)z_{i,i}(n+j)\mathbf{z}_{i,h}\mathbf{z}_{i,h}^{\mathrm{T}}\right]\mathbf{f}_j \\ &+ \frac{\Omega^2}{\overline{\gamma}_i}\|\mathbf{f}_j\|^2. \end{aligned} \tag{3.4}$$

Using [1, Lemma 1] for the fourth order moment of a Gaussian process, the previous result can be written as

$$\begin{aligned}\mathcal{E}\{\hat{\alpha}_h^2\alpha_i^2\} &= \mathbf{f}_j^{\mathrm{H}}\Big(\mathcal{E}[z_{r,i}(n+j)z_{r,i}(n+j)]\mathcal{E}[\mathbf{z}_{r,h}\mathbf{z}_{r,h}^{\mathrm{T}}] \\ &+ \mathcal{E}[z_{r,i}(n+j)\mathbf{z}_{r,h}]\mathcal{E}[z_{r,i}(n+j)\mathbf{z}_{r,h}^{\mathrm{T}}] \\ &+ \mathcal{E}[z_{r,i}(n+j)\mathbf{z}_{r,h}^{\mathrm{T}}]\mathcal{E}[z_{r,i}(n+j)\mathbf{z}_{r,h}]\Big)\mathbf{f}_j \\ &+ \mathbf{f}_j^{\mathrm{H}}\Big(\mathcal{E}[z_{i,i}(n+j)z_{i,i}(n+j)]\mathcal{E}[\mathbf{z}_{r,h}\mathbf{z}_{r,h}^{\mathrm{T}}] \\ &+ \mathcal{E}[z_{i,i}(n+j)\mathbf{z}_{r,h}]\mathcal{E}[z_{i,i}(n+j)\mathbf{z}_{r,h}^{\mathrm{T}}] \\ &+ \mathcal{E}[z_{i,i}(n+j)\mathbf{z}_{r,h}^{\mathrm{T}}]\mathcal{E}[z_{i,i}(n+j)\mathbf{z}_{r,h}]\Big)\mathbf{f}_j \\ &+ \mathbf{f}_j^{\mathrm{H}}\Big(\mathcal{E}[z_{r,i}(n+j)z_{r,i}(n+j)]\mathcal{E}[\mathbf{z}_{i,h}\mathbf{z}_{i,h}^{\mathrm{T}}] \\ &+ \mathcal{E}[z_{r,i}(n+j)\mathbf{z}_{i,h}]\mathcal{E}[z_{r,i}(n+j)\mathbf{z}_{i,h}^{\mathrm{T}}] \\ &+ \mathcal{E}[z_{r,i}(n+j)\mathbf{z}_{i,h}^{\mathrm{T}}]\mathcal{E}[z_{r,i}(n+j)\mathbf{z}_{i,h}]\Big)\mathbf{f}_j \\ &+ \mathbf{f}_j^{\mathrm{H}}\Big(\mathcal{E}[z_{i,i}(n+j)z_{i,i}(n+j)]\mathcal{E}[\mathbf{z}_{i,h}\mathbf{z}_{i,h}^{\mathrm{T}}] \\ &+ \mathcal{E}[z_{i,i}(n+j)\mathbf{z}_{i,h}]\mathcal{E}[z_{i,i}(n+j)\mathbf{z}_{i,h}^{\mathrm{T}}] \\ &+ \mathcal{E}[z_{i,i}(n+j)\mathbf{z}_{i,h}^{\mathrm{T}}]\mathcal{E}[z_{i,i}(n+j)\mathbf{z}_{i,h}]\Big)\mathbf{f}_j \\ &+ \frac{\Omega^2}{\overline{\gamma}_i}\|\mathbf{f}_j\|^2. \end{aligned} \tag{3.5}$$

Introducing the notation $z_i(n) = x_1 + \jmath y_1$ and $z_h(n) = x_2 + \jmath y_2$, the following assumption is used:

$$\begin{aligned}\rho_{z,st} &= \frac{\mathcal{E}[z_i(n+\tau)z_h^*(n)]}{\Omega} \\ &\triangleq \frac{\mathcal{E}[z_i(n)z_h^*(n)]}{\Omega} \cdot \frac{\mathcal{E}[z_i(n+\tau)z_i^*(n)]}{\Omega} \\ &= \rho_{z,s} \cdot \rho_{z,t}, \end{aligned} \tag{3.6}$$

where $\rho_{z,s}$ and $\rho_{z,t}$ are the normalized correlation coefficients between complex Gaussians in space and time, respectively. This implies that

$$\mathcal{E}[z_i(n+\tau)z_h^*(n)] = \rho_{z,s} \cdot \mathcal{E}[z_i(n+\tau)z_i^*(n)]. \tag{3.7}$$

Using the Jakes model, $\rho_{z,t}$ is real and $\mathcal{E}[z_i(n+\tau)z_i^*(n)] = \Omega \cdot J_0(2\pi f_D \tau)$ [2]. In terms of its real and imaginary parts, $\rho_{z,st}$ may then also be written as [3, Appendix A]

$$\begin{aligned}\rho_{z,st} &= \frac{\mathcal{E}[z_i(n+\tau)z_h^*(n)]}{\Omega} \\ &= \frac{\mathcal{E}[(x_1+\jmath y_1)(x_2-\jmath y_2]}{\Omega} \\ &= \frac{\mathcal{E}[x_1x_2] + \mathcal{E}[y_1y_2] + \jmath(\mathcal{E}[x_2y_1] - \mathcal{E}[x_1y_2])}{\Omega} \\ &= \frac{2\mathcal{E}[x_1x_2] - \jmath 2\mathcal{E}[x_1y_2]}{\Omega} \\ &= \rho_{z,s} \cdot \rho_{z,t} = (c - \jmath d) \cdot \rho_{z,t}, \end{aligned} \tag{3.8}$$

where c and d are the normalized real and imaginary parts of $\rho_{z,s}$, respectively. Hence,

$$\mathcal{E}[x_1x_2] = \mathcal{E}[y_1y_2] = c \cdot \frac{\Omega}{2} J_0(2\pi f_D \tau) \tag{3.9}$$

$$\mathcal{E}[x_1y_2] = -\mathcal{E}[x_2y_1] = d \cdot \frac{\Omega}{2} J_0(2\pi f_D \tau). \tag{3.10}$$

Now, expressions included in (3.5) may be written

$$\mathcal{E}[z_{r,i}(n+j)\mathbf{z}_{r,h}] = \mathcal{E}[z_{i,i}(n+j)\mathbf{z}_{i,h}] = c \cdot \frac{\Omega}{2}\mathbf{r}_j \tag{3.11}$$

$$\mathcal{E}[z_{r,i}(n+j)\mathbf{z}_{i,h}] = -\mathcal{E}[z_{i,i}(n+j)\mathbf{z}_{r,h}] = d \cdot \frac{\Omega}{2}\mathbf{r}_j \tag{3.12}$$

where $\mathbf{r}_j = \frac{1}{\Omega}\mathcal{E}[\mathbf{z}_h z_h^*(n+j)]$. An element $[\mathbf{r}_j]_k$ of $\mathbf{r}_j$ will be function of the lag τ between the relevant pilot symbol time instant $n-kL$ and of the time $n+j$ of the CSNR to be predicted only. Finally, the following result is obtained:

$$\begin{aligned}
\mathcal{E}\{\hat{\alpha}_h^2 \alpha_i^2\} &= \mathbf{f}_j^{\mathrm{H}} \left(\frac{\Omega^2}{4}\mathbf{R} + 2c^2 \frac{\Omega^2}{4}\mathbf{r}_j \mathbf{r}_j^{\mathrm{T}} \right) \mathbf{f}_j + \mathbf{f}_j^{\mathrm{H}} \left(\frac{\Omega^2}{4}\mathbf{R} + 2d^2 \frac{\Omega^2}{4}\mathbf{r}_j \mathbf{r}_j^{\mathrm{T}} \right) \mathbf{f}_j \\
&+ \mathbf{f}_j^{\mathrm{H}} \left(\frac{\Omega^2}{4}\mathbf{R} + 2d^2 \frac{\Omega^2}{4}\mathbf{r}_j \mathbf{r}_j^{\mathrm{T}} \right) \mathbf{f}_j + \mathbf{f}_j^{\mathrm{H}} \left(\frac{\Omega^2}{4}\mathbf{R} + 2c^2 \frac{\Omega^2}{4}\mathbf{r}_j \mathbf{r}_j^{\mathrm{T}} \right) \mathbf{f}_j \\
&+ \frac{\Omega^2}{\overline{\gamma}_i} \|\mathbf{f}_j\|^2 \\
&= \Omega^2 \mathbf{f}_j^{\mathrm{H}} \mathbf{R} \mathbf{f}_j + \frac{\Omega^2}{\overline{\gamma}_i} \|\mathbf{f}_j\|^2 + (c^2 + d^2)\Omega^2 \mathbf{f}_j^{\mathrm{H}} \mathbf{r}_j \mathbf{r}_j^{\mathrm{T}} \mathbf{f}_j \\
&= \Omega^2 r + \rho_s \Omega^2 |\mathbf{f}_j^{\mathrm{H}} \mathbf{r}_j|^2, \qquad (3.13)
\end{aligned}$$

where $r = \mathbf{f}_j^{\mathrm{H}} \mathbf{R} \mathbf{f}_j + \frac{1}{\overline{\gamma}_i}\|\mathbf{f}_j\|^2$ [4, Appendix], $\mathbf{R} = \frac{1}{\Omega}\mathrm{Cov}(\mathbf{z}_h, \mathbf{z}_h) = \frac{1}{\Omega}\mathcal{E}[\mathbf{z}_h \mathbf{z}_h^{\mathrm{H}}]$, and $c^2 + d^2 = |\rho_{z,s}|^2 = \rho_s$ is the spatial power correlation coefficient [3].

References

[1] H. Holm, "Adaptive coded modulation and channel estimation tools for flat fading channels," Ph.D. dissertation, The Norwegian University of Science and Technology, April 2002 (available at: http://www.tele.ntnu.no/projects/beats/theses.htm).

[2] G. L. Stüber, *Principles of Mobile Communications*. Second edition, Kluwer Academic Publishers, 2001.

[3] M. O. Hasna, M. -S. Alouini, and M. K. Simon, "Effect of fading correlation on the outage probability of cellular mobile radio systems," *in Proc. IEEE Vehicular Technology Conference*, vol. 3, pp. 1794–1798, October 2001.

[4] G. E. Øien, H. Holm, and K. J. Hole, "Impact of channel prediction on adaptive coded modulation performance in Rayleigh fading," *IEEE Transactions on Vehicular Technology*, vol. 53, no. 3, pp. 758–769, May 2004.

Appendix 4

ASE and average BER under idealized assumptions

In this Appendix, expressions for the ASE and the average BER are derived under idealized assumptions, i.e., perfect channel knowledge and zero delay on the feedback channel. In this case, the predicted CSNR $\hat{\gamma} = \gamma$, and $\rho = 1$. The bivariate gamma distribution in (B.10) may then be exchanged for the exact/approximate PDF of γ. This is done in order to validate the accuracy of the approximate PDF. Note that in the following, the results are in general derived for identically distributed and spatially correlated Nakagami-m fading channels. The results for Rayleigh fading channels are obtained by letting $m = 1$.

Exact PDF

Let $\{\gamma_h\}_{h=1}^{H}$ be a set of H correlated and identically distributed gamma variates $\gamma_h \sim \mathcal{G}(m, \overline{\gamma}_h/m)$. The exact PDF of the combined CSNR at the output of an MRC receiver is then equal to [1, Eq. (5)]

$$f_\gamma(\gamma) = \prod_{h=1}^{H} \left(\frac{\lambda_1}{\lambda_h}\right)^m \sum_{k=0}^{\infty} \delta_k \cdot \frac{\gamma^{Hm+k-1} e^{-\gamma/\lambda_1}}{\lambda_1^{Hm+k} \Gamma(Hm+k)}, \tag{4.1}$$

where $\lambda_1 = \min_h\{\lambda_h\}$. The set $\{\lambda_h\}_{h=1}^{H}$ contains the eigenvalues of the matrix $\mathbf{A} = \mathbf{DC}$, where $\mathbf{D}$ is a $H \times H$ diagonal matrix with entries $\{\overline{\gamma}_h/m\}_{h=1}^{H}$, and $\mathbf{C}$ is a $H \times H$ positive definite matrix defined by

$$\mathbf{C} = \begin{bmatrix} 1 & \sqrt{\rho_{12}} & \cdots & \sqrt{\rho_{1H}} \\ \sqrt{\rho_{21}} & 1 & \cdots & \sqrt{\rho_{2H}} \\ \vdots & \vdots & \ddots & \vdots \\ \sqrt{\rho_{H1}} & \cdots & \cdots & 1 \end{bmatrix}. \tag{4.2}$$

The coefficients δ_k can be obtained recursively by the formula [1, Eq. (7)]

$$\delta_{k+1} = \frac{m}{k+1} \sum_{i=1}^{k+1} \left[\sum_{h=1}^{H} \left(1 - \frac{\lambda_1}{\lambda_h} \right)^i \right] \cdot \delta_{k+1-i}, \tag{4.3}$$

for $k = 0, 1, 2, \ldots$, and $\delta_0 = 1$. For a constant correlation model, $\lambda_1 = \lambda_2 = \ldots = \lambda_{H-1}$, and when inserting for the eigenvalues [1, Eq. (12)], the inner sum of (4.3) may be simplified to

$$\sum_{h=1}^{H} \left(1 - \frac{\lambda_1}{\lambda_h} \right)^i = \left(\frac{\sqrt{\rho_s} H}{1 + \sqrt{\rho_s}(H-1)} \right)^i. \tag{4.4}$$

With the aid of [2, Eq. (C.1)], the average BER when code n is applied, $\overline{\mathrm{BER}}_n$, is equal to

$$\overline{\mathrm{BER}}_n = a_n \prod_{h=1}^{H} \left(\frac{\lambda_1}{\lambda_h} \right)^m \sum_{k=0}^{\infty} \frac{\delta_k}{(\lambda_1 \mu_n)^\alpha} \left[\overline{\Gamma}(\alpha, \gamma_n \mu_n) - \overline{\Gamma}(\alpha, \gamma_{n+1} \mu_n) \right], \tag{4.5}$$

where $\alpha = Hm + k$, and $\mu_n = \frac{b_n \lambda_1 + M_n}{M_n \lambda_1}$. The probability of selecting code n, P_n, is given by the expression

$$P_n = \prod_{h=1}^{H} \left(\frac{\lambda_1}{\lambda_h} \right)^m \sum_{k=0}^{\infty} \delta_k \left[\overline{\Gamma}(\alpha, \gamma_n / \lambda_1) - \overline{\Gamma}(\alpha, \gamma_{n+1} / \lambda_1) \right]. \tag{4.6}$$

The ASE and average BER may then be derived from (B.41) and (B.44) respectively, where $R_n = \log_2(M_n) - 1/2$ is the information rate of code n. For numerical evaluation, the infinite sums are truncated to S terms. Denoting the truncated version of the PDF in (4.1) as $f_\gamma(\gamma, S)$, the error of the area under the PDF due to truncation can be obtained as [3]

$$I_e(S) = 1 - \int_0^\infty f_\gamma(\gamma, S) d\gamma = 1 - c \sum_{k=0}^{S} \delta_k, \tag{4.7}$$

where $c = \prod_{h=1}^{H} \left(\frac{\lambda_1}{\lambda_h} \right)^m$. In this paper, the infinite sums are terminated at $S = 260$ terms. For the number of antennas and correlation values used in the numerical examples, $I_e(S)$ is then less than 10^{-3} in all cases.

Approximate PDF

When the rate-adaptive system is operating on correlated Nakagami-m fading channels, an approximate PDF of the combined CSNR at the output of the MRC receiver may be written as [4]

$$p_\gamma(\gamma) = \frac{\gamma^{m_d - 1} e^{-\gamma/\theta}}{\theta^{m_d} \Gamma(m_d)}. \tag{4.8}$$

Using this PDF, the average BER when code n is applied, $\overline{\mathrm{BER}}_n$, is equal to

$$\overline{\mathrm{BER}}_n = \frac{a_n}{(\theta\nu_n)^{m_d}} \left[\overline{\Gamma}(m_d, \gamma_n\nu_n) - \overline{\Gamma}(m_d, \gamma_{n+1}\nu_n)\right], \tag{4.9}$$

where $\nu_n = \frac{b_n\theta + M_n}{M_n\theta}$. The probability of selecting code n, P_n, is given by

$$P_n = \overline{\Gamma}(m_d, \gamma_n/\theta) - \overline{\Gamma}(m_d, \gamma_{n+1}/\theta). \tag{4.10}$$

The ASE and average BER may then be derived from (B.41) and (B.44) respectively, where $R_n = \log_2(M_n) - 1/2$ is the information rate of code n.

References

[1] M. -S. Alouini, A. Abdi, and M. Kaveh, “Sum of gamma variates and performance of wireless communication systems over Nakagami-fading channels,” *IEEE Transactions on Vehicular Technology*, vol. 50, no. 6, pp. 1471–1479, November 2001.

[2] H. Holm, “Adaptive coded modulation and channel estimation tools for flat fading channels,” Ph.D. dissertation, The Norwegian University of Science and Technology, April 2002 (available at: http://www.tele.ntnu.no/projects/beats/theses.htm).

[3] T. A. Tran and A. B. Sesay, “Distribution of the sum of arbitrarily correlated gamma variates and performance of MRC over Nakagami-*m* fading channels,” *submitted to IEEE Transactions on Vehicular Technology*.

[4] C. Mun, C. -H. Kang, and H. -K. Park, “Approximation of SNR statistics for MRC diversity systems in arbitrarily correlated Nakagami fading channels,” *IEE Electronics Letters*, vol. 35, no. 4, pp. 266–267, February 1999.

Appendix 5

Comments on the results in [1]

In [1, Fig. 1], the curves for the exact distribution are correct, but they do not correspond to the analytical result in [1, Eq. (8)]. In order to reproduce the same set of curves as depicted in [1, Fig. 1], ρ^2 in [1, Eq. (8)] must be replaced by ρ. Then, [1, Eq. (8)] is in accordance with related results reported in the literature [2, Eq. (D.14)], [3, Eq. (5)], [4, Eq. (18)].

In addition, we believe that the covariance matrix in [1, Eq. (9)] should be redefined, so that the entries outside the main diagonal become complex correlation coefficients, since **R** originally is defined as the normalized covariance matrix between complex fading amplitudes. This change leads to a new set of curves for the approximate distribution in [1, Fig. 1]. In [5], closed-form expressions for m_d based on complex covariance matrices are derived (reproduced as ψ in Table B.1), from which the corrected approximate PDF curves can be computed from [1, Eq. (7)] and [1, Eq. (3)]. In Figure 5.1, a new set of curves for the approximate PDF (denoted corrected) are compared to the original ones in [1, Fig. 1].

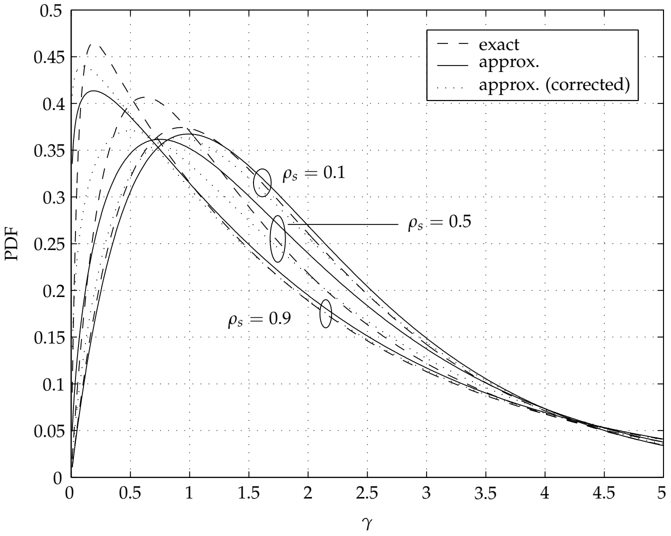

FIGURE 5.1: Comparison of the exact and approximate PDFs in [1, Fig. 1], including corrected results based on a complex representation of the covariance matrix in [1, Eq. (9)]. The curves are obtained for $\overline{\gamma} = 1$ and $m = 1$.

References

[1] C. Mun, C. -H. Kang, and H. -K. Park, "Approximation of SNR statistics for MRC diversity systems in arbitrarily correlated Nakagami fading channels," *IEE Electronics Letters*, vol. 35, no. 4, pp. 266–267, February 1999.

[2] H. Holm, "Adaptive coded modulation and channel estimation tools for flat fading channels," Ph.D. dissertation, The Norwegian University of Science and Technology, April 2002 (available at: http://www.tele.ntnu.no/projects/beats/theses.htm).

[3] M. -S. Alouini, A. Abdi, and M. Kaveh, "Sum of gamma variates and performance of wireless communication systems over Nakagami-fading channels," *IEEE Transactions on Vehicular Technology*, vol. 50, no. 6, pp. 1471–1479, November 2001.

[4] V. A. Aalo, "Performance of maximal-ratio diversity systems in a correlated Nakagami-fading environment," *IEEE Transactions on Communications*, vol. 43, no. 8, pp. 2360–2369, August 1995.

[5] B. Holter and G. E. Øien, "On the amount of fading for MIMO diversity systems," *accepted for publication in IEEE Transactions on Wireless Communications*.

Appendix 6

Proof of the Amount of Fading expression in (D.11)

Using a mathematical model assuming that the transmit and receive correlation properties are decoupled in a MIMO diversity system operating on identically distributed spatially correlated Nakagami-m channels, the amount of fading may be expressed as

$$\mathrm{AF} = \frac{\sum_{j=1}^{n_T} \|\mathbf{t}_j\|^2 \sum_{i=1}^{n_R} \|\mathbf{r}_i\|^2}{N^2 m}, \tag{6.1}$$

where $\| \cdot \|^2$ denotes the squared Euclidean vector norm, m is the common fading parameter of all the channels, n_T denotes the number of transmit antennas, n_R denotes the number of receive antennas, and $N = n_T \cdot n_R$. The vectors $\mathbf{t}_j$ and $\mathbf{r}_i$ denote rows j and i of the transmit and receive correlation matrices, respectively.

Proof: Let Λ represent the diagonal eigenvalue matrix of the complex correlation matrix $\mathbf{R}_H$. Assuming decoupled correlation properties at the receiver and transmitter, the correlation matrix $\mathbf{R}_H$ may be written as $\mathbf{R}_H = \mathbf{R}_{Tx} \otimes \mathbf{R}_{Rx}$, where the symbol $\otimes$ denotes the Kronecker product, and the matrices $\mathbf{R}_{Tx}$ and $\mathbf{R}_{Rx}$ denote the decoupled transmit and receive correlation matrices, respectively. Due to multiplicative properties of the eigenvalues of matrices in a Kronecker product, the nominator in (D.10) may be decomposed into the product $\mathrm{tr}(\Lambda_{Tx}^2)\mathrm{tr}(\Lambda_{Rx}^2)$, where Λ_{Tx} and Λ_{Rx} are the diagonal eigenvalue matrices of $\mathbf{R}_{Tx}$ and $\mathbf{R}_{Rx}$, respectively. The following chain of equalities can then be obtained for the transmitter part:

$$\mathrm{tr}(\Lambda_{Tx}^2) = \mathrm{tr}(\mathbf{R}_{Tx}^2) = \sum_{j=1}^{n_T} (\mathbf{R}_{Tx}\mathbf{R}_{Tx})_{jj} = \sum_{j=1}^{n_T}\sum_{k=1}^{n_T} t_{jk} \cdot t_{kj} \overset{(i)}{=} \sum_{j=1}^{n_T}\sum_{k=1}^{n_T} t_{jk} \cdot t_{jk}^* = \sum_{j=1}^{n_T} \|\mathbf{t}_j\|^2, \tag{6.2}$$

where t_{jk} denotes a single entry at the jth row and kth column of $\mathbf{R}_{Tx}$, and $\mathbf{t}_j$ denotes the jth row of $\mathbf{R}_{Tx}$. The equality (i) is true since a correlation matrix is Hermitian symmetric. A similar chain of equalities can be obtained for the receiver part, resulting in

$$\mathrm{tr}(\Lambda_{Rx}^2) = \mathrm{tr}(\mathbf{R}_{Rx}^2) = \sum_{i=1}^{n_R} \|\mathbf{r}_i\|^2, \tag{6.3}$$

where $\mathbf{r}_i$ denotes the ith row of $\mathbf{R}_{Rx}$. □

Appendix 7

An alternative expression for the determinant of a constant correlation matrix

A constant correlation matrix $\mathbf{R}$ of size $L \times L$ is called a Lth order intraclass correlation matrix if it has the following structure [1]

$$\mathbf{R} = \begin{bmatrix} a & b & b & \cdots & b \\ b & a & b & \cdots & b \\ b & b & a & \cdots & b \\ \vdots & \vdots & \vdots & \ddots & \vdots \\ b & b & b & \cdots & a \end{bmatrix}, \tag{7.1}$$

with $b \geq -a/(L-1)$. By normalizing this matrix, 1s are obtained on the main diagonal and the factor b/a off the main diagonal. Denoting $x = b/a$ and assuming that $x \in [0,1]$, a closed-form expression for the determinant of $\mathbf{R}$ may be written as [2]

$$\det(\mathbf{R}) = (1-x)^{L-1}(1 + x(L-1)). \tag{7.2}$$

Due to the normalized main diagonal and the fact that the variable x is confined to the finite interval range $x \in [0,1]$, we have observed (depicted in Figure D.1) that the cumulative distribution function (CDF) of a beta distributed RV can be used in an alternative expression for the determinant given in (7.2). The alternative expression may be derived as follows.

The probability distribution function (PDF) of a beta distributed RV with free parameters $\alpha > 0$ and $\beta > 0$ is given by [3]

$$betapdf(x) = \frac{\Gamma(\alpha+\beta)}{\Gamma(\alpha)\Gamma(\beta)}(1-x)^{\beta-1}x^{\alpha-1}. \tag{7.3}$$

The CDF can then be expressed as

$$betacdf(x;\alpha,\beta) = \int_0^x \frac{\Gamma(\alpha+\beta)}{\Gamma(\alpha)\Gamma(\beta)}(1-u)^{\beta-1}u^{\alpha-1}du. \tag{7.4}$$

Evaluating the function $f(x,\alpha,\beta) = 1 - betacdf(x;\alpha,\beta)$ when $\alpha = 2$, the following result is obtained:

$$\begin{aligned} f(x,2,\beta) &= 1 - betacdf(x;2,\beta) = 1 - \int_0^x \frac{\Gamma(\beta+2)}{\Gamma(\beta)}(1-u)^{\beta-1}udu \\ &= 1 - \frac{\Gamma(\beta+2)}{\Gamma(\beta)}\left[\frac{1-(1-x)^{\beta}(1+\beta x)}{\beta(\beta+1)}\right] \\ &= (1-x)^{\beta}(1+\beta x). \end{aligned} \tag{7.5}$$

By comparison, (7.5) and (7.2) represent identical expressions by selecting $\beta = L - 1$. Hence, the determinant of a constant correlation matrix $\mathbf{R}$ can be written as

$$\det(\mathbf{R}) = 1 - betacdf(x;2,L-1). \tag{7.6}$$

Since the parameter β must be larger than zero, this expression is valid only when $L \geq 2$. The CDF of a beta distributed RV is equal to the regularized beta function $I(\cdot;\cdot,\cdot)$ [4], and the determinant can also be written as

$$\det(\mathbf{R}) = 1 - betacdf(x;2,L-1) = 1 - I(x;2,L-1) = I(1-x;L-1,2), \tag{7.7}$$

where $I(x;\alpha,\beta) = 1 - I(1-x;\beta,\alpha)$ [5]. Hence,

$$\det(\mathbf{R}) = betacdf(1-x;L-1,2). \tag{7.8}$$

References

[1] M. K. Simon and M. -S. Alouini, *Digital Communication over Fading Channels: A Unified Approach to Performance Analysis*. John Wiley & Sons, Inc., 2000.

[2] S. J. Press, *Applied Multivariate Analysis: Using Bayesian and frequentist methods of inference*. Holt, Rinehart, Winston, 2nd edition, 1972.

[3] M. H. DeGroot and M. J. Schervish, *Probability and Statistics*. Addison-Wesley, 2002.

[4] http://mathworld.wolfram.com.

[5] http://functions.wolfram.com.

Appendix 8

Proofs of statistical results presented in Paper E

Feedback load

Given the mode of operation of the SET, SETps and SWT multiuser access schemes, the number of probed users per time-slot before channel access N_e when operating on i.i.d. channels is a discrete RV whose PMF is given by

$$P[N_e = k] = \begin{cases} p^{k-1} \cdot (1-p) & k = 1, 2, \ldots, K-1 \\ p^{K-1} & k = K \\ 0 & \text{otherwise} \end{cases} \tag{8.1}$$

Using this PMF, the mean of N_e is equal to

$$\mu_{N_e} = \frac{1 - p^K}{1 - p}. \tag{8.2}$$

Proof: The mean of N_e may in general be written as

$$\mu_{N_e} = (1-p) \sum_{k=1}^{K-1} k p^{k-1} + K p^{K-1}. \tag{8.3}$$

An expression for the finite sum in (8.3) can be obtained by taking the derivative of an existing sum identify in [1, Appendix A], leading to the following relation:

$$\sum_{k=1}^{K-1} k p^{k-1} = \frac{1 - p^K - K p^{K-1}(1-p)}{(1-p)^2}, \tag{8.4}$$

for $p \neq 1$. Hence,

$$\mu_{N_e} = (1-p) \cdot \frac{1 - p^K - Kp^{K-1}(1-p)}{(1-p)^2} + Kp^{K-1} = \frac{1-p^K}{1-p}.$$

□

Using the PMF in (8.1), the variance of N_e is equal to

$$\sigma^2_{N_e} = \frac{p - (2K-1)p^K + (2K-1)p^{K+1} - p^{2K}}{(1-p)^2}. \tag{8.5}$$

Proof: The variance of N_c is expressed as

$$\begin{aligned} \sigma^2_{N_e} &= \mathcal{E}\{N_e^2\} - \mu^2_{N_e} \\ &= (1-p) \sum_{k=1}^{K-1} k^2 p^{k-1} + K^2 p^{K-1} - \mu^2_{N_e}. \end{aligned} \tag{8.6}$$

An expression for the finite sum in (8.6) can be obtained by taking the derivative of an existing sum identify in [1, Appendix A], leading to the following relation:

$$\sum_{k=1}^{K-1} k^2 p^{k-1} = \frac{1 + p - K^2 p^{K-1} + (2K^2 - 2K - 1)p^K - (K^2 - 2K + 1)p^{K+1}}{(1-p)^3}, \tag{8.7}$$

for $p \neq 1$. Hence,

$$\begin{aligned} \sigma^2_{N_e} &= (1-p) \cdot \frac{1 + p - K^2 p^{K-1} + (2K^2 - 2K - 1)p^K - (K^2 - 2K + 1)p^{K+1}}{(1-p)^3} \\ &+ K^2 p^{K-1} - \mu^2_{N_e} \\ &= \frac{p - (2K-1)p^K + (2K-1)p^{K+1} - p^{2K}}{(1-p)^2}. \end{aligned}$$

□

Waiting time

Given the mode of operation of the SWT multiuser access scheme, the number of coherence times N_c the BS has to wait before an acceptable user is found when operating on i.i.d. channels will be a discrete RV, with PMF:

$$P[N_c = t] = p^{Kt}(1 - p^K), \tag{8.8}$$

for $t = 0, 1, \ldots$. Using this PMF, the mean of N_c is equal to

$$\mu_{N_c} = \frac{p^K}{1 - p^K}. \tag{8.9}$$

Proof:

$$\mu_{N_c} = (1-p^K)\sum_{t=0}^{\infty} t p^{Kt} = (1-x)\sum_{t=0}^{\infty} t x^t = \frac{x}{1-x},$$

for $x = p^K < 1$ [2, Eq. (0.231)]. □

Using the PMF in (8.8), the variance of N_c is equal to

$$\sigma^2_{N_c} = \frac{p^K}{(1-p^K)^2}. \tag{8.10}$$

Proof:

$$\begin{aligned}
\sigma^2_{N_c} &= \mathcal{E}\{N_c^2\} - \mu^2_{N_c} \\
&= (1-p^K)\sum_{t=0}^{\infty} t^2 p^{Kt} - \mu^2_{N_c} \\
&= (1-x)\sum_{t=0}^{\infty} t^2 x^t - \mu^2_{N_c} \\
&= \frac{x(1+x)}{(1-x)^2} - \frac{x^2}{(1-x)^2} \\
&= \frac{x}{(1-x)^2},
\end{aligned}$$

for $x = p^K < 1$ [1, Appendix A]. □

References

[1] A. Ambardar, *Analog and Digital Signal Processing*. PWS Publishing Company, 1995.

[2] I. S. Gradshteyn and I. M. Ryzhik, *Table of Integrals, Series, and Products*. 5th ed., San Diego, CA: Academic Press, 1994.

Appendix 9

The optimal weights of an MRC receiver by means of an eigenfilter approach

Maximum ratio combining (MRC) is an efficient spatial diversity strategy to reduce signal fluctuations caused by multipath propagation in wireless communications. Among several different spatial diversity techniques, MRC represents the optimal (in a maximum signal-to-noise ratio (SNR) sense) diversity scheme in the absence of interference.[1] However, it also represents the diversity scheme with the highest complexity, since it requires knowledge of all channel fading parameters. Despite its complexity, the MRC receiver is frequently utilized for analysis purposes as a benchmark receiver with which to compare other (less complex) spatial diversity schemes.

A narrowband, flat-fading, single-input multiple-output (SIMO) system with n_R receive antennas is considered. Using a complex baseband representation, the received signal s_i at antenna $i \in \{1, 2, \ldots, n_R\}$ may be expressed as

$$s_i = h_i x + n_i, \tag{9.1}$$

where x, h_i and n_i are all random variables denoting the transmitted signal, the channel observed at receive antenna i, and additive white Gaussian noise (AWGN) received at antenna i, respectively. In the following, we shall have a reason to make a distinction between the random variable h_i

---

[1] When interference is introduced, the optimal combining scheme is denoted an *optimum combiner*, maximizing the instantaneous received signal-to-interference plus noise ratio (SINR) [1], [2, Ch. 10].

and the realizations (outcomes) of h_i at certain instants in time, in order to later be able to explicitly refer to the instantaneous received SNR for the current observed channel. For that purpose, a discrete time index k will be introduced into the expression in (9.1). Denoting the transmitted signal at time index $k \in \{0, 1, \ldots\}$ by $x^{(k)}$, the received signal $s_i^{(k)}$ may then be written as

$$s_i^{(k)} = h_i^{(k)} x^{(k)} + n_i^{(k)}. \tag{9.2}$$

Note that $h_i^{(k)}$ represents a specific realization (outcome) of the random variable h_i and by assumption, $h_i^{(k)}$ is perfectly known by the receiver by the time it is observed. Using vector notation, the received array response vector at time instant k may be compactly written as

$$\mathbf{s}_k = \mathbf{h}_k x^{(k)} + \mathbf{n}_k, \tag{9.3}$$

where[2] $\mathbf{s}_k = [s_1^{(k)}, \ldots, s_{n_R}^{(k)}]^{\mathrm{T}}$, $\mathbf{h}_k = [h_1^{(k)}, \ldots, h_{n_R}^{(k)}]^{\mathrm{T}}$, and $\mathbf{n}_k = [n_1^{(k)}, \ldots, n_{n_R}^{(k)}]^{\mathrm{T}}$. The vector channel $\mathbf{h}_k$ may be looked upon as a single realization of a random channel vector $\mathbf{h}$ (multivariate random variable) with possibly correlated entries. Depending on the radio propagation environment, various multipath fading models may be used to characterize the statistical behavior of the fading envelopes in $\mathbf{h}$. However, in this letter, a specific choice of fading model for each of the fading envelopes in the set $\{|h_i|\}_{i=1}^{n_R}$ is not needed, since the results are not influenced by such a selection. In the following, the optimal weights of an MRC receiver are obtained by means of an eigenfilter approach.

An MRC receiver represents a linear combiner, and the output y may in general be expressed as

$$\begin{aligned} y &= \mathbf{w}^{\mathrm{H}} \mathbf{s} && (9.4) \\ &= \mathbf{w}^{\mathrm{H}} \mathbf{h} x + \mathbf{w}^{\mathrm{H}} \mathbf{n}, && (9.5) \end{aligned}$$

where $\mathbf{w} \in \mathbb{C}^{n_R}$ are the (as yet unknown) weights of the linear combiner.[3] With an average power constraint $P_T = \mathcal{E}\{|x|^2\}$ at the transmitter, the instantaneous received signal power S at the output of the MRC receiver at time instant k can be expressed as

$$S = P_T \cdot \mathbf{w}^{\mathrm{H}} \mathbf{h}_k \mathbf{h}_k^{\mathrm{H}} \mathbf{w}. \tag{9.6}$$

---

[2] The superscript $(\cdot)^{\mathrm{T}}$ denotes matrix transpose.

[3] The superscript $(\cdot)^{\mathrm{H}}$ denotes Hermitian transpose and $\mathbb{C}$ denotes the set of complex numbers. The notation $\mathbb{C}^n$ denotes the set of complex-valued vectors of length n.

Recall that $\mathbf{h}_k$ represents a specific realization (outcome) of the random variable $\mathbf{h}$ observed at time instant k and that by assumption, $\mathbf{h}_k$ is perfectly known by the receiver by the time it is observed. The output noise power N may be expressed as

$$N = \mathcal{E}\{|\mathbf{w}^{\mathrm{H}}\mathbf{n}|^2\} = \mathbf{w}^{\mathrm{H}}\mathbf{R}_n\mathbf{w}, \tag{9.7}$$

where $\mathbf{R}_n = \mathcal{E}\{\mathbf{n}\mathbf{n}^{\mathrm{H}}\}$ denotes the noise covariance matrix.[4] Using (9.6) and (9.7), the instantaneous SNR at the output of the MRC receiver at time instant k, $\gamma_{mrc}^{(k)}$, can be expressed as

$$\gamma_{mrc}^{(k)} = \frac{S}{N} = \frac{P_T \cdot \mathbf{w}^{\mathrm{H}}\hat{\mathbf{R}}_k\mathbf{w}}{\mathbf{w}^{\mathrm{H}}\mathbf{R}_n\mathbf{w}}, \tag{9.8}$$

where $\hat{\mathbf{R}}_k = \mathbf{h}_k\mathbf{h}_k^{\mathrm{H}}$ denotes an estimate of the channel covariance matrix at time instant k. The optimization problem is now to determine the coefficient vector $\mathbf{w}$ so as to maximize (9.8) for the current observed channel vector $\mathbf{h}_k$.

Equal noise power

In the following, we assume equal noise power at each of the branches, and also that the noise is uncorrelated between the branches. This means that the noise correlation matrix introduced in the previous section can be represented as $\mathbf{R}_n = \sigma^2\mathbf{I}$, where σ^2 represents the noise power common to all branches and $\mathbf{I}$ represents the identity matrix. Taking the *conjugate derivative* $\partial/\partial\mathbf{w}^*$ [3] of (9.8) with respect to the weight vector $\mathbf{w}$, we obtain the following set of implications:

$$\begin{aligned} \frac{\partial\gamma_{mrc}^{(k)}}{\partial\mathbf{w}^*} &= 0 \\ &\Updownarrow \\ P_T \cdot \hat{\mathbf{R}}_k\mathbf{w}(\sigma^2\mathbf{w}^{\mathrm{H}}\mathbf{w}) &= \sigma^2\mathbf{w}(P_T \cdot \mathbf{w}^{\mathrm{H}}\hat{\mathbf{R}}_k\mathbf{w}) \\ &\Downarrow \\ \hat{\mathbf{R}}_k\mathbf{w} &= \left(\frac{\mathbf{w}^{\mathrm{H}}\hat{\mathbf{R}}_k\mathbf{w}}{\mathbf{w}^{\mathrm{H}}\mathbf{w}}\right)\mathbf{w}. \end{aligned} \tag{9.9}$$

Introducing $\lambda = \frac{\mathbf{w}^{\mathrm{H}}\hat{\mathbf{R}}_k\mathbf{w}}{\mathbf{w}^{\mathrm{H}}\mathbf{w}}$ and using the result of (9.9) in (9.8), we obtain

$$\gamma_{mrc}^{(k)} = \frac{P_T \cdot \mathbf{w}^{\mathrm{H}}\hat{\mathbf{R}}_k\mathbf{w}}{\sigma^2\mathbf{w}^{\mathrm{H}}\mathbf{w}} = \frac{P_T \cdot \mathbf{w}^{\mathrm{H}}\lambda\mathbf{w}}{\sigma^2\mathbf{w}^{\mathrm{H}}\mathbf{w}} = \frac{P_T \cdot \lambda}{\sigma^2}. \tag{9.10}$$

---

[4] $\mathcal{E}\{\cdot\}$ denotes the statistical average.

It can be seen that the maximum value of the output SNR is given as $\frac{P_T \cdot \lambda_{max}}{\sigma^2}$, where λ_{max} is the largest eigenvalue of the matrix $\hat{\mathbf{R}}_k$. The optimal weight vector that yields the maximum output SNR is thus given by the eigenvector associated with λ_{max}. To obtain a non-trivial solution of (9.9), $\mathbf{w}$ must reside within the column space (range) of $\hat{\mathbf{R}}_k$, denoted $\mathcal{R}(\hat{\mathbf{R}}_k)$. Since all the columns in $\hat{\mathbf{R}}_k$ are linear combinations of the single vector $\mathbf{h}_k$, it is a rank one matrix and $\mathcal{R}(\hat{\mathbf{R}}_k) = \{\mathbf{h}_k\}$. Since $\mathcal{R}(\hat{\mathbf{R}}_k)$ consists of just a single vector, the only way of obtaining a non-trivial solution is to select $\mathbf{w}_{opt} = c \cdot \mathbf{h}_k$ for an arbitrary $c \neq 0$. Inserting this result into the left side of (9.9), we obtain

$$||\mathbf{h}_k||^2 c \cdot \mathbf{h}_k = \lambda_{max} \mathbf{w}_{opt}. \tag{9.11}$$

The maximum eigenvalue is thus identified as $\lambda_{max} = ||\mathbf{h}_k||^2$. Using this result in (9.10), the maximum output SNR is given by

$$\gamma_{mrc}^{(k)} = \frac{P_T \cdot ||\mathbf{h}_k||^2}{\sigma^2} = \sum_{i=1}^{n_R} \frac{P_T \cdot |h_i^{(k)}|^2}{\sigma^2} = \sum_{i=1}^{n_R} \gamma_i^{(k)} , \tag{9.12}$$

where $|h_i^{(k)}|$ and $\gamma_i^{(k)} = \frac{P_T \cdot |h_i^{(k)}|^2}{\sigma^2}$ denote the fading envelope and the instantaneous SNR at the ith branch at time index k, respectively. This result confirms that the output SNR may be expressed as a sum of the SNR values from the individual branches, which is a specific feature of the MRC receiver [4].

Unequal noise power

With unequal noise power in the diversity branches, the SNR expressed in (9.8) can not be simplified. Taking the conjugate derivative of (9.8) with respect to the weight vector $\mathbf{w}$, we obtain the following set of implications:

$$\begin{aligned} \frac{\partial \gamma_{mrc}^{(k)}}{\partial \mathbf{w}^*} &= 0 \\ &\Updownarrow \\ P_T \cdot \hat{\mathbf{R}}_k \mathbf{w} (\mathbf{w}^{\mathrm{H}} \mathbf{R}_n \mathbf{w}) &= (P_T \cdot \mathbf{w}^{\mathrm{H}} \hat{\mathbf{R}}_k \mathbf{w}) \mathbf{R}_n \mathbf{w} \\ &\Downarrow \\ \hat{\mathbf{R}}_k \mathbf{w} &= \left(\frac{\mathbf{w}^{\mathrm{H}} \hat{\mathbf{R}}_k \mathbf{w}}{\mathbf{w}^{\mathrm{H}} \mathbf{R}_n \mathbf{w}} \right) \mathbf{R}_n \mathbf{w}. \end{aligned} \tag{9.13}$$

Introducing $\lambda = \frac{\mathbf{w}^{\mathrm{H}} \hat{\mathbf{R}}_k \mathbf{w}}{\mathbf{w}^{\mathrm{H}} \mathbf{R}_n \mathbf{w}}$ and exploiting the fact that $\mathbf{R}_n$ is nonsingular (diagonal matrix with all entries $\sigma_i^2 > 0$), (9.13) may be expressed as

$$\mathbf{R}_n^{-1} \hat{\mathbf{R}}_k \mathbf{w} = \lambda \mathbf{w}. \tag{9.14}$$

The optimal weight vector is now the eigenvector of the matrix $\mathbf{R}_n^{-1}\hat{\mathbf{R}}_k = \mathbf{R}_n^{-1}\mathbf{h}_k\mathbf{h}_k^{\mathrm{H}}$ corresponding to the largest eigenvalue of the same matrix. By letting $\mathbf{h}_k' = \mathbf{R}_n^{-1}\mathbf{h}_k$, the current eigenvalue problem may be expressed as

$$\hat{\mathbf{R}}_k'\mathbf{w} = \lambda\mathbf{w}, \tag{9.15}$$

where $\hat{\mathbf{R}}_k' = \mathbf{h}_k'\mathbf{h}_k^{\mathrm{H}}$. A non-trivial solution of this equation is obtained if $\mathbf{w}$ resides within the column space of $\hat{\mathbf{R}}_k'$, denoted $\mathcal{R}(\hat{\mathbf{R}}_k')$. Every matrix of the simple form $\mathbf{h}_k'\mathbf{h}_k^{\mathrm{H}}$ has rank one [5] and the column space $\mathcal{R}(\hat{\mathbf{R}}_k') = \{\mathbf{h}_k'\}$. As in the previous section, the only choice to obtain a non-trivial solution is to select $\mathbf{w}_{opt} = c \cdot \mathbf{h}_k'$ for an arbitrary $c \neq 0$. Inserting this result into the left side of (9.15), we obtain

$$\mathbf{h}_k^{\mathrm{H}}\mathbf{R}_n^{-1}\mathbf{h}_k c \cdot \mathbf{h}_k' = \lambda_{max}\mathbf{w}_{opt}, \tag{9.16}$$

and the maximum eigenvalue can be identified as $\lambda_{max} = \mathbf{h}_k^{\mathrm{H}}\mathbf{R}_n^{-1}\mathbf{h}_k$. Inserting the optimal weight vector $\mathbf{w}_{opt} = c \cdot \mathbf{h}_k' = c \cdot \mathbf{R}_n^{-1}\mathbf{h}_k$ into (9.8), we obtain

$$\gamma_{mrc}^{(k)} = P_T \cdot \mathbf{h}_k^{\mathrm{H}}\mathbf{R}_n^{-1}\mathbf{h}_k = \sum_{i=1}^{n_R} \frac{P_T \cdot |h_i^{(k)}|^2}{\sigma_i^2} = \sum_{i=1}^{n_R} \gamma_i^{(k)}, \tag{9.17}$$

where $\gamma_i^{(k)} = \frac{P_T \cdot |h_i^{(k)}|^2}{\sigma_i^2}$. As in the previous subsection, the output SNR may be expressed as the sum of the SNR values from the individual branches.

To summarize, we have obtained the following optimal weights:

$$\mathbf{w}_{opt} \propto \begin{cases} \mathbf{h}_k & \text{Equal noise power} \\ \mathbf{R}_n^{-1}\mathbf{h}_k & \text{Unequal noise power} \end{cases} \tag{9.18}$$

Using these optimal weights, the output SNR from a MRC receiver may be expressed as

$$\gamma_{mrc}^{(k)} = \begin{cases} \frac{P_T \cdot \|\mathbf{h}_k\|^2}{\sigma^2} & \text{Equal noise power} \\ P_T \cdot \mathbf{h}_k^{\mathrm{H}}\mathbf{R}_n^{-1}\mathbf{h}_k & \text{Unequal noise power} \end{cases} \tag{9.19}$$

Looking at the inner product in (9.4), the actual weights used in the inner product are the complex conjugate of the weights presented in (9.18). The optimal weights are then in agreement with the result presented in [4]. Since the solutions in this section is linked to an eigenvalue problem, the optimal (spatial) filter obtained using this method is commonly called an eigenfilter. As noted in [3], the optimum filter characterized in this way may be viewed as the stochastic counterpart of a matched filter.

References

[1] J. H. Winters, "Optimum combining in digital mobile radio with co-channel interference," *IEEE Transactions on Vehicular Technology*, vol. VT-33, no. 3, pp. 144–154, August 1984.

[2] M. K. Simon and M.-S. Alouini, *Digital Communication over Fading Channels: A Unified Approach to Performance Analysis*. John Wiley & Sons, Inc., 2000.

[3] S. Haykin, *Adaptive filter theory*. Prentice Hall, Inc., 2001.

[4] D. G. Brennan, "Linear diversity combining techniques," *in Proc. IRE*, vol. 47, pp. 1075–1102, 1959.

[5] G. Strang, *Linear algebra and its applications*. Harcourt Brace Jovanovich, Inc., 1988.